Overstory dynamics regulate the spatial variability in forest-floor CO_2 fluxes across a managed boreal forest landscape

Eduardo Martínez-García [a,*], Mats B. Nilsson [a], Hjalmar Laudon [a], Tomas Lundmark [a], Johan E.S. Fransson [b,c], Jörgen Wallerman [b], Matthias Peichl [a]

[a] Department of Forest Ecology and Management, Swedish University of Agricultural Sciences, Skogsmarksgränd 17, SE-901 83, Umeå, Sweden
[b] Department of Forest Resource Management, Swedish University of Agricultural Sciences, Skogsmarksgränd 17, SE-901 83, Umeå, Sweden
[c] Department of Forestry and Wood Technology, Linnaeus University, Georg Lückligs väg 1, SE-351 95, Växjö, Sweden

ARTICLE INFO

ABSTRACT

The forest-floor represents an important interface for various carbon dioxide (CO_2) fluxes, however, our knowledge of their variability and drivers across a managed boreal forest landscape is limited. Here, we used a three-year (2016−2018) data set of biometric- and chamber-based flux measurements to investigate the net forest-floor CO_2 exchange (NE_{ff}) and its component fluxes across 50 forest stands spanning different soil types, tree species, and age classes within a 68 km^2 boreal catchment in Sweden. We found that the forest-floor acted as a net CO_2 source with the 10th–90th percentile (used hereafter for describing reported variations) ranging from 149 to 399 g C m^{-2} yr^{-1}. Among the key landscape attributes, stand age strongly affected most NE_{ff} component fluxes, whereas tree species and soil type effects were weak and absent, respectively. Specifically, forest-floor net CO_2 emissions increased with stand age due to declining understory gross and net primary production, ranging between 77–275 and 49–163 g C m^{-2} yr^{-1}, respectively. Furthermore, we observed higher understory production rates in pine than in spruce stands. Across the 50 stands, the total forest-floor respiration ranged between 340 and 549 g C m^{-2} yr^{-1} and its spatial variation was primarily regulated by its autotrophic components, i.e., understory and tree root respiration, which displayed divergent increasing and decreasing age-related trends, respectively. Furthermore, heterotrophic soil respiration remained within a relatively narrow range (154–290 g C m^{-2} yr^{-1}), possibly owing to compensating gradients in forest-floor properties. We further identified tree biomass as the major driver of the landscape-scale variations of CO_2 fluxes, likely attributable to modulating effects on forest-floor resource availability and growing conditions. This implies that tree growth responses to forest management and global change will be particularly important for regulating magnitudes and spatial variations of forest-floor CO_2 fluxes in boreal forests.

1. Introduction

The boreal forest region covers 12.5 ± 1.5 million km^2 (Dixon et al., 1994) accounting for 27% of the global forested area, and storing about one-third of the global terrestrial carbon (Pan et al., 2011). Thus, boreal forest landscapes play an important role in the global carbon cycle and provide a large potential for mitigating global warming (Beer et al., 2010). Our understanding of the magnitude and spatio-temporal variations of the net ecosystem carbon exchange in boreal forests has developed rapidly due to a growing network of eddy covariance flux-stations during recent decades (Baldocchi, 2014; Campioli et al., 2016; Luyssaert et al., 2007). However, considerable uncertainties

remain regarding the partitioning of the carbon exchange into the overstory tree canopy and the forest-floor components. Specifically, knowledge on the role and contributions of the forest-floor carbon dioxide (CO_2) fluxes and their underlying drivers is currently limited, which hampers our understanding of boreal forest carbon cycling and our ability to predict its response to future changes in climate and management strategies.

The net forest-floor CO_2 exchange (NE_{ff}) is comprised of a complex balance of various component fluxes (Fig. 1), including the gross primary production of the understory vegetation (GPP_u), comprised of various functional types (i.e., ericaceous dwarf shrubs, mosses, herbs, and lichens), and the total forest-floor respiration (R_{ff}; Chapin et al.,

2006). R_{ff} is further composed of various metabolic processes associated with the autotrophic respiration of understory plants (RA_u) and tree roots (RA_{tr}) along with the heterotrophic soil respiration (RH) by microorganisms decomposing litter and soil organic matter (Chapin et al., 2006). The difference between GPP_u and RA_u regulates the net primary production of understory vegetation (NPP_u; Chapin et al., 2006). Given the separate drivers underlying these various fluxes, their magnitudes and relative importance in regulating NE_{ff} likely differ considerably in both time and space.

Previous site-level studies suggest that the magnitudes of both the production and respiration fluxes as well as their relative contributions to the ecosystem carbon balance of boreal forests vary largely. For instance, the contribution of GPP_u to the ecosystem GPP has been reported to vary between 3 and 61% (Bergeron et al., 2009; Chi et al., 2021; Ikawa et al., 2015; Kolari et al., 2006; Misson et al., 2007). Furthermore, NPP_u has been shown to account for about 20–50% of the ecosystem NPP (Nilsson and Wardle, 2005). Likewise, R_{ff} may contribute between 40 and 70% of the ecosystem respiration (Chi et al., 2021; Ikawa et al., 2015; Launiainen et al., 2005; Misson et al., 2007). At present, it remains a challenge to reconcile these large ranges in the relative importance of forest-floor CO_2 fluxes reported in previous studies, which imply multiple processes at work. This includes large uncertainties with respect to the soil-vegetation interactions among the different sources of forest-floor respiration (i.e., RA_u, RA_{tr}, and RH). Specifically, it remains unclear whether these reported differences in forest-floor CO_2 fluxes among individual sites are the result from the span in their geographical and climatic locations or a function of landscape heterogeneity.

Key landscape attributes including edaphic (i.e., soil type) and structural (i.e., tree species and stand age) properties differ across a managed forest landscape. Most boreal forests in Fennoscandia occur on either poorly sorted glacial till or well sorted glaciofluvial sediments (Stroeven et al., 2016). Compared to the sediment soils found in valley fills and fluvial systems, till soils are present in upslope topographic positions and, therefore, characterized by a lower mineral soil depth, pH, clay content, and water retention as well as thicker organic horizon and higher nutrient availability (Marek and Richardson, 2020). Furthermore, Scots pine (*Pinus sylvestris* L.) and Norway spruce (*Picea abies* (L.) H. Karst.) are the dominant overstory tree species in these high latitudes (Holmström et al., 2018). Compared to spruce, pine dominates in stands with a drier soil-moisture regime and more nutrient-poor soils. In addition, the relative sparse canopy architecture of pine trees allows for a higher fraction of available light reaching the forest-floor, which leads to a more abundant understory communities (Barbier et al., 2008; Kumar et al., 2018a). In contrast, spruce stands are associated with higher tree biomass and litter production and therefore thicker soil organic layers (Barbier et al., 2008; Hedwall et al., 2013; Petersson et al., 2019).

Apart from variations in both soil types and dominant tree species, a mosaic of highly fragmented forest stands encompassing different ages further increases the complexity across the managed boreal forest landscape in Fennoscandia (Kuuluvainen and Gauthier, 2018). For instance, tree, soil, litter, and dead wood carbon pools gradually increase with stand age (Goulden et al., 2011; Pregitzer and Euskirchen, 2004), whereas an opposite trend is identified for understory vegetation (Barbier et al., 2008). In addition, forest stand development leads to changes in forest-floor environment including age-related declines in light availability, soil and air temperature as well as soil moisture (Barbier et al., 2008; Hiltbrunner et al., 2012; Palmroth et al., 2019). Stand age also exhibits direct effects on different soil properties such as increasing soil C:N ratio (Hume et al., 2016; Makita et al., 2016) and/or decreasing bulk density (Chen and Shrestha, 2012).

In boreal forests, the few studies of GPP_u dynamics suggest that its spatial variability depends on understory biomass, species composition, and photosynthetic activity in response to light availability and air temperature (e.g., Bergeron et al., 2009; Kolari et al., 2006; Kulmala et al., 2011). However, the nature and extent to which these various controls in concert regulate GPP_u is uncertain. Furthermore, even though similar controls may drive spatial variations in NPP_u, their regulation across the boreal landscape, especially for its belowground component, is also poorly resolved. In contrast, extensive effort has been directed towards understanding the controls on the spatial variability in RH in forest ecosystems, encompassing soil temperature and moisture, litter inputs, quantity and quality of soil organic matter, and/or soil microbial activity as major drivers (Bond-Lamberty et al., 2004; Curiel Yuste et al., 2007; Harmon et al., 2011; Hursh et al., 2017). Nonetheless, a comprehensive assessment of the variability in RH within the context of the multiple controls imposed by landscape heterogeneity in northern latitudes is lacking.

At present, it is known that vegetation controls the autotrophic forest-floor respiration (RA_{ff}) directly through its carbon allocation patterns, understory and tree root biomass, and indirectly via its effects on hydrological processes and below-canopy environment conditions (Davidson and Janssens, 2006; Högberg et al., 2009; Kulmala et al.,
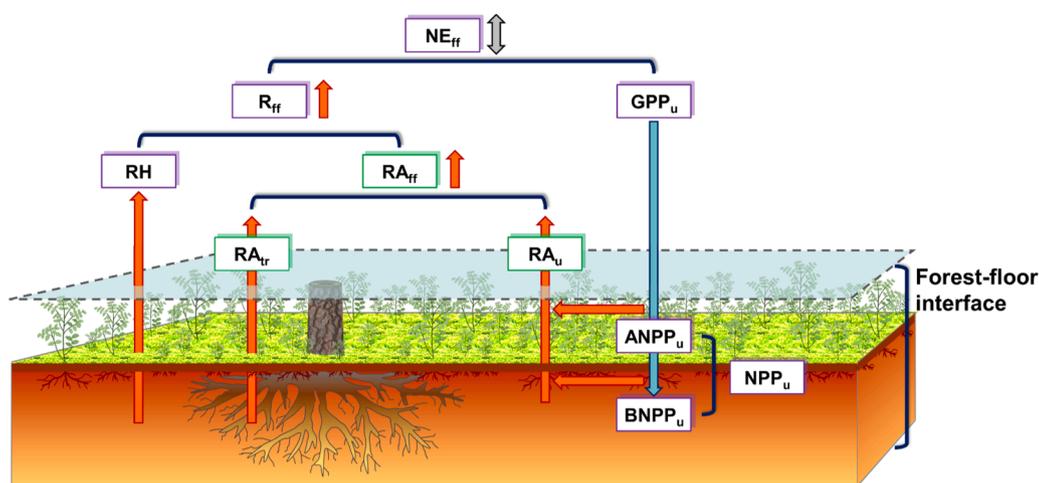

Fig. 1. Schematic representation of the major components of the forest-floor CO_2 exchange. Note that subscript u refers to understory vegetation, subscript tr refers to tree roots, and subscript ff refers to the entire forest-floor system including soil, tree roots, and understory vegetation. $ANPP_u$ and $BNPP_u$: aboveground and belowground net primary production of understory vegetation, respectively (their sum is indicated as NPP_u), RA_u and RA_{tr}: autotrophic respiration of understory vegetation (including both above- and belowground components) and tree roots, respectively (their sum is indicated as RA_{ff}), RH: heterotrophic soil respiration, GPP_u: gross primary production of understory vegetation ($GPP_u = NPP_u + RA_u$), R_{ff}: total forest-floor respiration ($R_{ff} = RA_{ff} + RH$), and NE_{ff}: net forest-floor CO_2 exchange ($NE_{ff} = R_{ff} – GPP_u$). Blue arrow indicates carbon uptake, orange arrows indicate carbon release, whereas gray arrow indicates that both carbon uptake and release can occur. In this study, fluxes within the purple boxes were directly measured, whereas fluxes within the green boxes were indirectly estimated.

2009; Vargas et al., 2011). However, the specific controls of its two components, i.e. RA_u and RA_{tr}, have rarely been compared within a boreal landscape. Altogether, given the vast range in biotic and abiotic conditions and their potential for altering the various production and respiration fluxes, detailed knowledge about NE_{ff} dynamics in boreal forests is lacking. This limits our understanding of contributions from forest-floor fluxes to the ecosystem carbon balance and hampers our ability to evaluate future global change impacts on the boreal forest carbon cycle.

In this study, we use a three-year (2016−2018) data set that aggregates biometric- and chamber-based flux measurements of forest-floor CO_2 fluxes across a boreal forest landscape in northern Sweden. Data were collected in 50 forest stands encompassing different soil types (sediment vs. till), dominant tree species (pine vs. spruce), and age classes (from initiation to old-growth stands). Our specific objectives were to: 1) investigate the variability in the net forest-floor CO_2 exchange and its individual component fluxes across a managed boreal forest landscape, 2) examine their sensitivity to landscape attributes including edaphic (soil type) and structural (tree species and stand age) properties, and 3) determine the key biotic and abiotic factors modulating their variability at the landscape-scale.

2. Materials and methods

2.1. Study area and experimental design

The study was conducted within the Krycklan Catchment Study (KCS, Laudon et al., 2021), a multi-scale long-term monitored catchment spanning 68 km^2 and located *ca.* 50 km northwest of Umeå (Sweden, 64°14′N, 19°46′E; Fig. 2). The climate conditions are cold temperate humid (Laudon et al., 2021), with a 30-year (1991−2020) average annual air temperature of 2.4 ± 0.8 °C (here and hereafter, "±" denotes one standard deviation) and average annual precipitation sum of 638 ± 107 mm, where about 30% of it falls as snow. The catchment has a gently undulating terrain, with elevation ranging from 138 to 339 m.a.s.

l. The upper elevations of the KCS are dominated by forest on glacial-till soils (58% of the total area) with presence of mires (9%), whereas the lower elevations are represented by forested areas on glaciofluvial sediment soils (30% of the total area). Lakes (1%) and arable land/built areas (2%) cover the remaining area. A complex mosaic of forest stands in different age classes covers 87% of the total area, which are dominated by Scots pine (55%) and Norway spruce (23%), with scattered occurrence (9%) of birch (*Betula pendula* Roth. and *Betula pubescens* Ehrh.), alder (*Alnus incana* (L.) Moench.), and aspen (*Populus tremula* L.). The understory vegetation is dominated by ericaceous dwarf shrubs (mostly *Vaccinium myrtillus* L., *Vaccinium vitis-idaea* L. and *Empetrum nigrum* L.), with a ground layer of mosses (predominantly *Hylocomium splendens* (Hedw.) Br. Eur. and *Pleurozium schreberi* (Brid.) Mitt.), and lichens (*Cladonia* spp.).

Fifty forest stands spanning 5 to 211 years-old (average age of 73 ± 43 years) were selected by stratification based on a systematic regular grid of 556 permanent sample plots located over the entire catchment (Fig. 2). Within each selected stand, the sample plot (10 m radius) belonging to the KCS' plot-network was used for biometric- and chamber-based flux measurements (Supplementary Fig. S1). Stand age (i.e., number of years after stand establishment) was determined in each sample plot as the basal area-weighted average age obtained by coring 8−10 dominant trees outside each sample plot in 2015. Based on the quaternary deposits map of the Swedish Geological Survey, each stand was assigned to a soil parent material (hereafter "soil type"), i.e., sediment soils ($n = 15$) and till soils ($n = 35$). In addition, stands were also classified by dominant tree species (hereafter "tree species"), i.e., Scots pine ($n = 28$) and Norway spruce ($n = 22$), based on their basal area and tree density (see Supplementary materials, Section 1). Furthermore, we classified these stands into five age classes (hereafter "stand age"), i.e., Initiation ($n = 8$), Young ($n = 9$), Middle-aged ($n = 13$), Mature ($n = 14$) and Old-growth ($n = 6$), including stands ranging from 5−30, 31−60, 61−80, 81−110, and >130 years old, respectively.
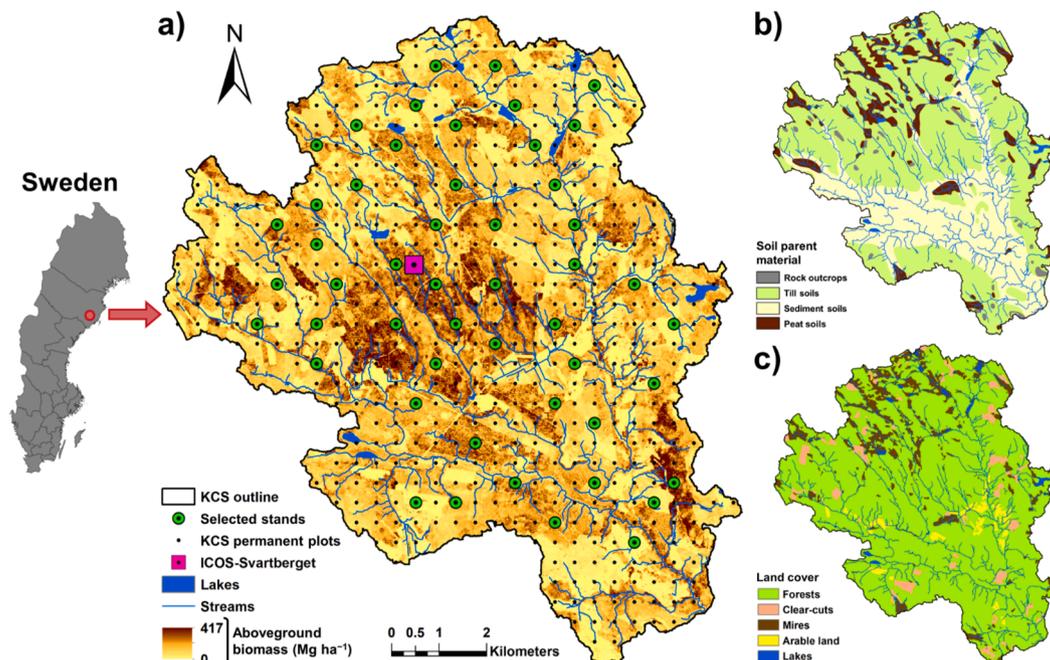

Fig. 2. Location map of the Krycklan Catchment Study (KCS) in northern Sweden. Detailed map a) displays the outline of the KCS, selected forest stands, KCS' network of permanent sample plots, ICOS-Svartberget (Integrated Carbon Observation System) Atmosphere-Ecosystem station along with the light detection and ranging (LiDAR) derived estimates of aboveground biomass (data obtained from the Swedish University of Agricultural Sciences and Swedish Forest Agency). Detailed maps b) and c) denote the soil parent material (i.e., quaternary deposits map; data obtained from the Swedish Geological Survey) and the land cover types (data obtained from the Swedish National Mapping Agency), respectively. Lakes and streams within the KCS are also shown.

2.2. Forest stand characteristics

2.2.1. Tree and dead wood biomass

We recorded location, species, diameter at breast height (DBH, 1.3 m), and height (H) for all living trees and standing dead trees (snags; assigned to decay class I (Sandström et al., 2007)) in April in 2016 and 2018 for each plot. Missing DBHs in April 2017 were derived from increment cores obtained from 75 representative trees of each species (selected by DBH size) over the 50 plots in April 2019. Saplings (DBH < 3 cm) were not included in the inventory, which total tree biomass was considered negligible. In October 2019, downed dead wood (logs) were also identified by species, measured for diameter and length, and assigned to a decay class (I−III, Sandström et al., 2007). Both aboveground and coarse root tree biomass was estimated using species-specific allometric equations as a function of DBH and H (Marklund, 1988; Petersson and Ståhl, 2006; Repola, 2008) and converted to carbon stocks (AGC_t and BGC_{t_cr}, respectively), assuming that carbon content of dry biomass was 50%. Belowground tree biomass carbon stock (BGC_t) was calculated as BGC_{t_cr} plus the fine root component (BGC_{t_fr}, see below). Biomass of snags was also estimated using the above-mentioned allometric equations, whereas the biomass of logs was estimated by multiplying their volume with their species- and decay class-specific wood densities (Sandström et al., 2007). Dead wood biomass carbon stocks (i.e., C_{dw-s} and C_{dw-l} for snags and logs, respectively) were calculated by using species-specific carbon concentrations for each decay class to convert dry biomass to carbon mass (Mäkinen et al., 2006; Sandström et al., 2007).

2.2.2. Aboveground understory and litter biomass

Aboveground understory biomass, containing different plant functional types (PFTs; lichens, herbs, mosses, and dwarf shrubs), was measured by clipping in six systematically arranged 0.25 m^2 quadrats per plot in 2017 (Supplementary Fig. S1; Aguinaga-Gil, 2018). Clipping was conducted in early summer (June, three quadrats) and during the peak growth (August, three quadrats). Shrubs were sorted by species and components (leaves and stems), while for lichens, herbs, and mosses all species were pooled together. Samples were oven-dried (60 °C, 48 h) and weighed. Aboveground understory biomass carbon stock (AGC_u) in 2017 was calculated as the averaged value between both samplings, assuming that 50% of dry biomass was carbon. AGC_u estimation in 2016 and 2018 is presented in Supplementary materials, Section 2. Furthermore, the litter standing on the forest-floor (i.e., leaf litter and fine woody debris) was also collected from the same quadrats, oven-dried (60 °C, 48 h) and weighed. Total litter biomass carbon stock (C_l) in 2017 was obtained by averaging values between June and August and assuming a carbon content of 50% in dry biomass. A mass-balance approach assuming steady-state conditions was used for the C_l estimation in 2016 and 2018 (Supplementary materials, Section 3).

2.2.3. Fine-root biomass

The fine-root biomass in the organic (O) and mineral (two depths: 0−10 cm [MS1] and 10−20 cm [MS2]) soil horizons was estimated in June 2017 via sequential coring. Three soil cores (Ø 10 cm and 5 cm for organic and mineral soils, respectively) were systematically collected per plot (Supplementary Fig. S1; Aguinaga-Gil, 2018). The depth of the O horizon (O_{depth}) was determined for each core. Cores were sieved through a 2 mm mesh and the remaining soil and rocks were saved. The volume of sieved rocks was determined by the water displacement method. Roots (Ø ≤ 2 mm) were manually removed from the soil, washed, oven-dried (60 °C, 48 h), and weighed. Fine-root biomass was related to the area sampled, converted to carbon mass (50% dry biomass), summed per horizons, and scaled-up to the plot to obtain the fine-root biomass carbon stock (BGC_{fr}) in 2017. The partitioning of BGC_{fr} into fine-roots of trees (BGC_{t_fr}) and understory vegetation (BGC_u) as well as their estimation in 2016 and 2018 are further described in Supplementary materials, Sections 4–5.

2.2.4. Organic and mineral soil carbon and nitrogen content

Sieved soil from sequential cores was pooled into one bulk sample per each soil horizon at each plot and oven-dried (60 °C, 48 h). Then, carbon and nitrogen concentrations of each horizon were estimated from a homogenised subsample on an elemental analyser (Flash EA 2000, Thermo Fisher Scientific, Bremen, Germany). We assumed a negligible change in carbon and nitrogen concentrations at each plot during 2016−2018. Soil organic carbon (SOC) of each horizon was estimated as (Eq. (1)):

$$SOC = \left[\left(\frac{C}{1000} \right) \times \left(\frac{H_{depth}}{100} \right) \times BD \times \left(\frac{100 - CRF}{100} \right) \right] \times 10 \qquad (1)$$

where C is the carbon mass fraction (‰), H_{depth} is the horizon depth (cm), BD is the soil bulk density (g cm^{-3}), CRF is the volumetric fraction of coarse inorganic fragments > 2 mm (i.e., rocks, stones, and boulders, %), and 10 is the factor for converting g C m^{-2} to Mg C ha^{-1}. Specifically, BD was estimated by pedotransfer functions following Nilsson and Lundin (2006). To obtain CRF, the relative volume of rocks was obtained from sieved samples (see SubSection 2.2.3), whereas the relative volume of stones and boulders was estimated to be 47.6% and 40.9% for till and sediment soils, respectively, following Stendahl et al. (2009). The total SOC stock was then derived as the sum of its total content at O, MS1, and MS2 horizons.

2.2.5. Total ecosystem carbon stock

Total ecosystem carbon stock (C_{total}, Mg C ha^{-1}) was determined during 2016−2018 according to Eq. (2):

$$C_{total} = C_t + C_u + C_{dw} + C_l + SOC \qquad (2)$$

where C_t is the total tree biomass carbon stock (i.e., $AGC_t + BGC_t$), C_u is the total understory biomass carbon stock (i.e., $AGC_u + BGC_u$), C_{dw} is the total dead wood biomass carbon stock (i.e., $C_{dw-s} + C_{dw-l}$), C_l is the total litter biomass carbon stock, and SOC is the total soil organic carbon stock up to 20 cm depth.

2.2.6. Ancillary vegetation measurements

Leaf area index at peak growing season (LAI_{max}, m^2 m^{-2}) was recorded on August 2017 at six systematic locations within each plot (Supplementary Fig. S1) using LAI-2200 method (Li-Cor, Lincoln, NE, USA). Additional LAI_{max} estimation in 2016 and 2018, determined by assuming a comparable relative annual change between LAI_{max} and tree stem biomass, is described in Supplementary materials, Section 6. In addition, understory vegetation properties such as photosynthetically active green tissue biomass (gtb, g m^{-2}; see Supplementary materials, Section 7) and phenological biomass development were also recorded. To track phenology, we used hourly images obtained by digital repeat photography to derive a vegetation greenness index based on the green chromatic coordinate (gcc, dimensionless; Sonnentag et al., 2012) for each image as (Eq. (3)):

$$gcc = DN_g / (DN_r + DN_g + DN_b) \qquad (3)$$

where DN_r, DN_g, and DN_b are the digital numbers (0–255) of the red, green and blue image channels within a selected region of interest as described in Peichl et al. (2015). More details on gcc estimation and normalization are given in Supplementary materials, Section 8.

2.2.7. Forest-floor environmental measurements

During each CO_2 flux sampling day (see SubSection 2.3.1.), below-canopy air temperature (Ta_{bc}, °C; handheld digital thermometer M514B, Sunartis, Mingle Instruments GmbH Europe, North Rhine-Westphalia, Germany) and photosynthetic photon flux density ($PPFD_{bc}$, µmol photons m^{-2} s^{-1}; quantum sensor QSO-S, Apogee Instruments Inc., Logan, UT, USA) were manually measured at each plot. Soil temperature at 10 cm depth (Ts_{10}, °C; previous thermometer) and

soil volumetric water content at 5 cm depth (SWC_5,%; moisture sensor GS3, METER Group Inc., Pullman, WA, USA) were also recorded at each plot. See Supplementary materials, Section 9 for additional information about sampling intervals and measurement points within each plot as well as the estimation of plot-level half-hourly values of Ta_{bc}, $PPFD_{bc}$, Ts_{10}, and SWC_5 during 2016–2018.

2.3. Net forest-floor CO₂ exchange and its component fluxes

2.3.1. Forest-floor CO₂ exchange

We established a split-plot design trenching experiment in late summer 2015, which was located 5 m outside from the sample plot boundary to avoid trampling disturbance. This set up included two adjacent subplots (1 m²), designated as vegetated (V) and vegetation removal and trenched (NV) subplots (Supplementary Fig. S1). The vegetated subplot was selected to include a vegetation cover and species composition representative for the entire plot. For each NV subplot, a trench of 10 cm width and 30–40 cm depth was dug around the subplot edges to exclude lateral root in-growth and thereafter at the beginning of each snow-free period (see Supplementary materials, Section 10 for the determination of snow-free and snow-covered periods during 2016−2018). The trenching was carried out in the preceding autumn and thus nearly 7 months before the beginning of CO₂ flux measurements in the following spring to reduce the effect of initially enhanced decomposition of residual roots in the NV subplots. In addition, understory vegetation within each trenched subplot was clipped and repeatedly thereafter whenever new shoots appeared. One square chamber base frame (aluminum, 0.2025 m², 0.05 m height) was embedded 1–2 cm into the soil surface in the center of each subplot to facilitate CO₂ flux measurements. The net forest-floor CO₂ exchange (NE_{ff}) and total forest-floor respiration (R_{ff}) were estimated on the vegetated subplots, while heterotrophic soil respiration (RH) was measured in the trenched subplots. Note that R_{ff} includes the contribution of autotrophic respiration of understory vegetation (RA_u) and tree roots (RA_{tr}) as well as RH (Fig. 1). The gross primary production of understory vegetation (GPP_u) was then derived as NE_{ff}–R_{ff}.

CO₂ fluxes (μmol CO₂ m⁻² s⁻¹) were measured with custom-made closed steady-state chamber (45 × 45 cm width, 20 cm height, 5 mm thick transparent acrylic Plexiglas® [Röhm GmbH, Weiterstadt, Hessen, Germany], 8% light attenuation [corrected for GPP_u estimates]). The chamber base had rims with a rubber gasket, ensuring an airtight chamber seal with base frame during the closure period. The chamber was connected to a portable infrared gas analyser (IRGA) in a closed sampling loop. During the study period, we used three different IRGAs (MI70, Vaisala, Helsinki, Finland; LGR-GGA-24EP, Los Gatos Research Inc., San Jose, CA, USA; GasScouterTM G4301, Picarro, Santa Clara, CA, USA). A cross-comparison among the three analysers suggested no significant differences in fluxes. Specifically, NE_{ff} was measured in ambient daylight, while for both R_{ff} and RH the chamber was covered with an opaque tarp to enable measurements under dark conditions. Fluxes were measured on a monthly basis at each plot from May to October during 2016−2018. Within each monthly sampling, 5–7 plots were measured per day between 8:00−16:00 h. A random order among the 50 plots was applied in each sampling to prevent diurnal effects. Measurements were performed across a wide range of daylight intensities at each plot over 3 snow-free periods to facilitate the development of plot-level light response curves for GPP_u. Additional information about calculation, data processing, quality control, and gap filling of fluxes is presented in Supplementary materials, Section 11.

GPP_u was described by a rectangular hyperbolic saturation light response curve (Thornley and Johnson, 1990) extended to include gcc as a proxy of the biomass phenology (Järveoja et al., 2016) and a temperature dependence function of photosynthesis (Collatz et al., 1992) (Eq. (4)):

$$GPP_u = \left(\frac{\alpha \times PPFD_{bc} \times A_{max} \times gcc_{subplot}}{\alpha \times PPFD_{bc} + \left(A_{max} \times gcc_{subplot} \right)} \right) \times \left(1 / \left(1 + e^{(s1 \times (T1-T))} \right) \right) \quad (4)$$

where GPP_u is the gross primary production of understory vegetation (μmol CO₂ m⁻² s⁻¹), α is the initial slope of the light-use efficiency of photosynthesis (mol CO₂ mol⁻¹ photons), $PPFD_{bc}$ is the below-canopy photosynthetic photon flux density (μmol photons m⁻² s⁻¹), A_{max} is the maximum photosynthesis at light saturation (μmol CO₂ m⁻² s⁻¹), $gcc_{subplot}$ is the normalized subplot-specific green chromatic coordinate, s1 and T1 determine the low-temperature inhibition, and T is the average of air and soil temperature (Ta_{bc} and Ts_{10}, respectively; °C). Here, T was defined according to Kulmala et al. (2019) with the aim to combine the specific effects of Ta_{bc} and Ts_{10} in regulating photosynthetic seasonality in boreal forests. As a preliminary step, s1 and T1 were first estimated by fitting Eq. (4) to $PPFD_{bc}$, $gcc_{subplot}$, and T on data pooled from all plots and sample dates ($n = 50$ plots × 3 years × 6 measurements). With the fixed s1 and T1, the remaining parameters (α and A_{max}) were then estimated for each plot by fitting again Eq. (4) including data pooled over all sample dates ($n = 3$ years × 6 measurements).

Respiration rates during the snow-free period (i.e., R_{ff_SF} and RH_{SF}) were modelled according to the Arrhenius temperature response function (Lloyd and Taylor, 1994) (Eq. (5)):

$$R_{SF} = R_{ref} \times e^{\left[E_0 \times \left(\left(\frac{1}{56.02} \right) - \left(\frac{1}{(Ts_{10} + 46.02)} \right) \right) \right]} \quad (5)$$

where R_{SF} refers to snow-free R_{ff} or RH (μmol CO₂ m⁻² s⁻¹), R_{ref} is ecosystem base respiration at 10 °C (μmol CO₂ m⁻² s⁻¹), E_0 is the parameter for activation energy (K⁻¹), and Ts_{10} is soil temperature at 10 cm depth (°C). Here, R_{ref} and E_0 were estimated for both R_{ff_SF} and RH_{SF} for each plot by fitting Eq. (5) to Ts_{10} including data pooled over all sample dates ($n = 18$). In addition, RH measurements performed in October were used to estimate RH during the snow-covered period (RH_{SC}). For this, Eq. (5) was fitted to Ts_{10} on data pooled from all plots ($n = 50$ plots × 3 years × 1 measurement). In this study, all coefficients in GPP_u, R_{ff}, and RH fluxes were estimated according to the Marquardt non-linear regression method. For all above CO₂ fluxes, see Supplementary materials for supporting information about model coefficients (Supplementary Tables S1−S4) and general modeling adjust (Supplementary Figs. S2−S3).

2.3.2. Net primary production of understory vegetation

Aboveground net primary production of understory vegetation ($ANPP_u$) in 2017 was estimated from the sum of biomass production of each individual PFT. Herbs production was evaluated from peak standing biomass in August, whereas production for lichens, mosses, and shrubs was calculated as their respective biomass increment between June and August. We then converted biomass to carbon using a factor of 0.5. $ANPP_u$ estimation in 2016 and 2018, determined from the annual shoot length increments (ASL, mm) in dwarf shrubs and assuming that the proportion between the different PFTs remained constant over the 3-year study period, is further described in Supplementary materials, Section 12. To estimate the belowground net primary production of fine roots ($BNPP_{fr}$), we used the ingrowth core method. Thus, the holes created after extraction of the sequential cores at each plot were widened to 10 cm Ø (Supplementary Fig. S1; Aguinaga-Gil, 2018). A plastic mesh core (Ø 10 cm, length 30 cm) was then inserted into each hole in June 2017, filled with sieved local root-free soil, and covered with leaf litter (1 cm thick layer). One core per plot was collected with a soil corer (Ø 10 cm) at the end of August 2017, while the two remaining were collected at the end of September 2018. On each sampling, cores were sieved through a 2 mm mesh and saved fine-roots (Ø < 2 mm) were oven-dried (60 °C, 48 h) and weighed. Fine-roots carbon content was assumed to be 50% of dry biomass. For this purpose, we first estimated

the daily fine-root production (FRP, g C m^{-2} day^{-1}) of each plot in 2017, which was derived from the total root biomass at the end of August 2017 divided by number of days of incubation in the field. To estimate the corrected plot-level fine-root production over the entire growing season, we multiplied daily FRP by the number of growing days ($n = 122$) between June and September 2017. Then, BNPP$_{fr}$ in 2018 was derived by subtracting fine-root production of September 2017 from September 2018. The partitioning of BNPP$_{fr}$ into fine-roots of trees (BNPP$_{t\,fr}$, data not shown) and understory vegetation (BNPP$_u$) as well as their estimation in 2016 and 2017 are described in Supplementary materials, Sections 13−15. Finally, the net primary production of understory vegetation (NPP$_u$) was derived as ANPP$_u$+BNPP$_u$.

2.3.3. Annual cumulative CO$_2$ fluxes

Half-hourly GPP$_u$, R$_{ff\_SF}$, RH$_{SF}$, and RH$_{SC}$ values were modelled using estimated α, A$_{max}$, s1, T1, R$_{ref}$, and E$_0$ along with PPFD$_{bc}$, T, Ts$_{10}$, and daily gcc$_{subplot}$ as input variables. In addition, half-hourly R$_{ff\,SC}$ was estimated as $1.09 \times$ RH$_{SC}$, which was based on the contribution of the autotrophic forest-floor respiration (RA$_{ff}$) during the snow-covered period in a similar boreal forest ecosystem (Pumpanen et al., 2015). Annual GPP$_u$, R$_{ff}$, and RH during 2016−2018 were then derived at plot-level from their cumulative sums. GPP$_u$ was determined at plot-level by using the ratio obtained between gtb measured in the vegetated subplot and the permanent sample plot (Supplementary materials, Section 7). Next, annual NE$_{ff}$ was calculated as R$_{ff}$−GPP$_u$. In addition, annual RA$_{ff}$ was derived as R$_{ff}$−RH, which in turn was partitioned into RA$_u$ (GPP$_u$−NPP$_u$) and RA$_{tr}$ (RA$_{ff}$−RA$_u$). Within this partitioning approach, NE$_{ff}$, GPP$_u$, NPP$_u$, ANPP$_u$, BNPP$_u$, R$_{ff}$, and RH are based on direct measurements from which RA$_{ff}$, RA$_u$, and RA$_{tr}$ are derived as indirect estimates (Fig. 1). In this study, all fluxes were presented as positive terms.

It is noteworthy that accounting for only the changes in NPP$_u$ likely led to a slightly over- and underestimation of RA$_u$ and RA$_{tr}$, respectively, during the last third of the snow-free period (i.e., September–October). Furthermore, the root trenching approach cannot separate RA from the fraction of RH resulting from the microbial metabolism of fresh root exudates (Bond-Lamberty et al., 2011). Our RH and RA$_{ff}$ estimates are, therefore, likely somewhat under- and overestimated, respectively. Finally, we note that due to the lack of data constraint, our modelled estimates potentially induced some bias during the period when the soil is snow covered. Nevertheless, our forest-floor respiration estimates during this period and their contribution to the annual flux (Supplementary Tables S5 and S6) were in agreement with findings from nearby boreal forests (Chi et al., 2021; Jocher et al., 2017).

2.4. Statistical analysis

Data sets of 3-year (2016–2018) mean annual values were tested prior to analysis for normality (Kolmogorov–Smirnov test) and homogeneity of variance (Levene's test) and log-transformed when necessary. One-way analysis of variance (ANOVA) was used to explore the effects from soil type, tree species, and stand age on biotic and abiotic factors as well as forest-floor CO$_2$ fluxes. Bonferroni *post hoc* test was used to further compare the means for significant differences ($p \leq 0.05$). The relative importance of biotic and abiotic factors in controlling each forest-floor CO$_2$ flux was examined using forward stepwise multiple linear regression (MLR) analysis ($p < 0.05$ threshold). The input set of potential biotic and abiotic explanatory factors included stand age, total biomass carbon stocks of tree, understory, dead wood, litter, and soil (C$_t$, C$_u$, C$_{dw}$, C$_l$, and SOC, respectively), forest-floor environmental conditions (Ta$_{bc}$, PPFD$_{bc}$, Ts$_{10}$, and SWC$_5$), and soil properties (O$_{depth}$, C:N ratio, and BD). All statistical analyses were conducted using the SPSS software (version 27.0; IBM corp., Armonk, NY, USA) and Statgraphics Centurion software (version XVI; StatPoint Technologies Inc., Warrenton, VA, USA).

3. Results

3.1. Spatial patterns of biotic and abiotic forest characteristics across a managed forest landscape

Across the 50 stands, basal area (BA) and leaf area index (LAI$_{max}$) ranged from 4.0 to 37.6 m^2 ha^{-1} and 0.9 to 5.0 m^2 m^{-2}, respectively (here and hereafter, the 10th and 90th percentiles define the reported "range"), with the latter showing higher values in till soil and spruce stands ($p < 0.05$, Table 1). Furthermore, both BA and LAI$_{max}$ significantly increased as stands aged ($p < 0.001$).

Three-year mean annual below-canopy air temperature (Ta$_{bc}$), light availability (PPFD$_{bc}$), soil temperature (Ts$_{10}$), and soil water content (SWC$_5$) varied widely across the 50 stands, ranging from 3.1 to 4.5 °C, 52 to 356 μmol photons m^{-2} m^{-2}, 2.5 to 5.4 °C, and 19.6 to 40.8%, respectively. Among them, only Ts$_{10}$ differed with tree species ($p < 0.05$), which was higher in pine than in spruce stands (Table 1). In addition, Ta$_{bc}$, PPFD$_{bc}$, and Ts$_{10}$ declined significantly with stand age ($p < 0.001$).

Soil properties such as depth of organic horizon (O$_{depth}$), C:N ratio, and bulk density (BD) were in the range 3.6–8.4 cm, 27.5–40.4 (dimensionless), and 0.60–1.05 g cm^{-3}, respectively. Specifically, higher O$_{depth}$ but lower BD were noted in till compared to sediment soils ($p < 0.01$, Table 1). Meanwhile, O$_{depth}$ was significantly higher in spruce compared to pine stands, whereas an opposite pattern was observed for C:N ratio and BD ($p < 0.05$).

Across the 50 stands, there was a 4–fold range in total ecosystem carbon stock (C$_{total}$, 41.0–161.3 Mg C ha^{-1}). The largest difference occurred in the tree biomass carbon stock (C$_t$) ranging from 7.1 to 110.6 Mg C ha^{-1}, which comprised on average 55% of C$_{total}$ (Supplementary Fig. S4). The remaining C$_{total}$ components including carbon stored in understory biomass (C$_u$), dead wood biomass (C$_{dw}$), litter biomass (C$_l$), and soil (SOC) carbon stocks were in the range 1.7–5.1, 0–6.1, 1.4–2.9, and 22.3–43.8 Mg C ha^{-1}, respectively. Moreover, C$_{total}$ and SOC were significantly higher in spruce than in pine stands ($p < 0.05$), whereas C$_u$ exhibited an opposite pattern ($p < 0.01$, Table 2). Furthermore, C$_{total}$ and most of its components increased significantly with stand age ($p < 0.05$), except for C$_u$, which decreased with age.

3.2. Magnitudes and spatial variability in forest-floor CO$_2$ fluxes

The forest-floor was a net CO$_2$ source in all 50 stands ranging from 149 to 399 g C m^{-2} yr^{-1}. No effect of soil type and tree species was apparent on the net forest-floor CO$_2$ exchange (NE$_{ff}$, $p = 0.81$ and 0.94, respectively). In contrast, NE$_{ff}$ increased significantly with stand age classes ($p < 0.01$) from 175 ± 76 to 326 ± 105 g C m^{-2} yr^{-1} from initiation to old-growth stands (Fig. 3, Supplementary Table S9). At the individual stand-level, NE$_{ff}$ was weakly negatively correlated to both the gross primary production of understory vegetation (GPP$_u$; Adj. R^2 = 0.26) and net primary production of understory vegetation (NPP$_u$, Adj. R^2 = 0.20; Fig. 4). In comparison, NE$_{ff}$ was more strongly positively correlated to the total forest-floor respiration (R$_{ff}$; Adj. R^2 = 0.45), which was primarily driven by a strong relationship with the tree root autotrophic respiration (RA$_{tr}$, Adj. R^2 = 0.68), whereas the correlation with the autotrophic respiration of understory vegetation (RA$_u$) was weaker (Adj. R^2 = 0.25). Meanwhile, the heterotrophic soil respiration (RH) did not explain any of the variation in NE$_{ff}$ (Adj. R^2 = 0.01).

Across the 50 stands, GPP$_u$ and NPP$_u$ varied from 77 to 275 and 49 to 163 g C m^{-2} yr^{-1}, respectively. Specifically, the variations in these production fluxes were not affected by soil type ($p = 0.41$ and 0.39 for GPP$_u$ and NPP$_u$, respectively). In contrast, higher GPP$_u$, NPP$_u$, and belowground net primary production of understory vegetation (BNPP$_u$) values (by 19, 20, and 29%, respectively) were found in pine than in spruce stands, although this result was only marginally significant for GPP$_u$ ($p = 0.054$, Fig. 3, Supplementary Table S9). In addition, stand age class significantly influenced GPP$_u$ as well as NPP$_u$ and its components (p

Table 1

Forest stand characteristics, forest-floor environmental conditions, and soil properties grouped according to key forest landscape attributes (i.e., soil type, tree species, and stand age). Age: basal area-weighted mean stand age (yr), BA: basal area ($m^2\ ha^{-1}$), LAI_{max}: leaf index at peak growing season ($m^2\ m^{-2}$), Ta_{bc}: average annual below-canopy air temperature (°C), $PPFD_{bc}$: average annual below-canopy instantaneous daytime photosynthetic photon flux density (μmol photons $m^{-2}\ s^{-1}$), Ts_{10}: average annual soil temperature at 10 cm depth (°C), SWC_5: average annual soil volumetric water content at 5 cm depth (%), O_{depth}: depth of the organic soil horizon (cm), C:N: average soil carbon-nitrogen ratio up to 20 cm depth (dimensionless), and BD: average soil bulk density up to 20 cm depth ($g\ cm^{-3}$). Values represent the 3-year (2016−2018) mean with standard deviation in brackets. Significant effects are marked in bold (see Supplementary Table S7 for further details). Different superscript letters denote significant differences (Bonferroni test, $p < 0.05$) for each main effect.

	Soil type		Tree species		Stand age				
Component	Sediment	Till	Pine	Spruce	Initiation	Young	Middle-aged	Mature	Old-growth
Age	58 (33)	80 (46)	69 (39)	79 (48)	**14 (9)[a]**	**48 (10)[b]**	**68 (5)[c]**	**92 (9)[d]**	**160 (27)[e]**
BA	17.3 (11.7)	22.2 (10.8)	19.4 (11.1)	22.5 (11.3)	**3.6 (3.0)[a]**	**17.5 (6.9)[b]**	**20.4 (6.0)[bc]**	**26.7 (7.7)[cd]**	**35.4 (6.5)[d]**
LAI_{max}	**2.1 (1.1)[a]**	**3.1 (1.5)[b]**	**2.2 (1.1)[a]**	**3.6 (1.5)[b]**	**0.8 (0.4)[a]**	**2.7 (1.1)[b]**	**2.8 (0.7)[b]**	**3.2 (1.1)[b]**	**4.7 (1.7)[c]**
Ta_{bc}	3.9 (0.6)	3.8 (0.6)	3.9 (0.6)	3.7 (0.6)	**4.7 (0.6)[b]**	**3.9 (0.3)[a]**	**3.7 (0.4)[a]**	**3.5 (0.5)[a]**	**3.7 (0.4)[a]**
$PPFD_{bc}$	229 (112)	178 (116)	208 (114)	175 (119)	**381 (48)[b]**	**184 (95)[a]**	**165 (77)[a]**	**161 (99)[a]**	**96 (49)[a]**
Ts_{10}	3.8 (1.2)	3.8 (1.0)	**4.1 (1.0)[b]**	**3.4 (1.1)[a]**	**5.6 (0.8)[b]**	**3.5 (0.4)[a]**	**3.8 (0.6)[a]**	**3.1 (0.8)[a]**	**3.4 (0.9)[a]**
SWC_5	28.1 (8.0)	29.9 (9.8)	27.4 (10.0)	31.9 (7.7)	22.3 (7.4)	29.0 (5.5)	31.5 (9.2)	31.1 (10.6)	30.7 (10.8)
O_{depth}	**4.5 (1.2)[a]**	**6.2 (2.0)[b]**	**5.1 (1.4)[a]**	**6.4 (2.3)[b]**	4.4 (1.2)	5.1 (1.7)	5.8 (2.1)	6.2 (1.8)	6.7 (2.7)
C:N	34.7 (5.7)	34.5 (4.9)	**35.9 (4.7)[b]**	**32.8 (5.1)[a]**	36.3 (5.8)	33.7 (5.2)	33.1 (4.3)	36.1 (5.0)	33.0 (5.7)
BD	**0.95 (0.13)[b]**	**0.80 (0.17)[a]**	**0.89 (0.11)[b]**	**0.78 (0.22)[a]**	0.93 (0.14)	0.94 (0.13)	0.79 (0.17)	0.81 (0.16)	0.79 (0.24)

Table 2

Carbon stocks ($Mg\ C\ ha^{-1}$) grouped according to key forest landscape attributes (i.e., soil type, tree species, and stand age). C_{total}: total ecosystem, C_t: total tree biomass, C_u: total understory biomass, C_{dw}: total dead wood biomass, C_l: total litter biomass, and SOC: soil organic carbon up to 20 cm depth. Values represent the 3-year (2016−2018) mean with standard deviation in brackets. Significant effects are marked in bold (see Supplementary Table S8 for further details). Different superscript letters denote significant differences (Bonferroni test, $p < 0.05$) for each main effect.

	Soil type		Tree species		Stand age				
Component	Sediment	Till	Pine	Spruce	Initiation	Young	Middle-aged	Mature	Old-growth
C_{total}	87.2 (48.3)	110.2 (44.4)	**91.8 (38.0)[a]**	**118.0 (52.4)[b]**	**38.4 (8.2)[a]**	**80.1 (23.6)[b]**	**103.7 (22.4)[bc]**	**130.2 (35.5)[cd]**	**161.3 (42.2)[d]**
C_t	51.4 (41.1)	70.0 (40.3)	55.8 (35.4)	75.4 (45.8)	**6.1 (4.8)[a]**	**47.0 (21.1)[b]**	**61.7 (18.2)[bc]**	**87.2 (28.4)[cd]**	**121.2 (39.1)[d]**
C_u	3.6 (1.0)	3.2 (1.5)	**3.8 (1.2)[b]**	**2.7 (1.3)[a]**	**4.8 (0.7)[b]**	**3.2 (1.0)[ab]**	**3.5 (1.4)[ab]**	**2.8 (1.2)[a]**	**2.2 (1.2)[a]**
C_{dw}	1.7 (3.3)	2.4 (2.9)	1.8 (2.8)	2.7 (3.2)	0.2 (0.2)	1.4 (1.6)	2.6 (2.1)	3.2 (4.6)	2.9 (2.3)
C_l	1.9 (0.7)	2.1 (0.5)	2.1 (0.6)	2.1 (0.6)	**1.4 (0.3)[a]**	**2.1 (0.5)[b]**	**2.0 (0.3)[b]**	**2.4 (0.7)[b]**	**2.4 (0.5)[b]**
SOC	28.6 (7.3)	32.5 (8.5)	**28.3 (5.7)[a]**	**35.1 (9.5)[b]**	**25.9 (5.3)[a]**	**26.4 (3.0)[a]**	**33.9 (9.4)[b]**	**34.6 (8.5)[b]**	**32.6 (8.7)[ab]**

< 0.05). Specifically, GPP_u and NPP_u declined from 263 ± 42 and $154 \pm 16\ g\ C\ m^{-2}\ yr^{-1}$, respectively, in initiation stands to 107 ± 38 and $71 \pm 22\ g\ C\ m^{-2}\ yr^{-1}$, respectively, in old-growth stands.

R_{ff} ranged from 340 to 549 $g\ C\ m^{-2}\ yr^{-1}$ without significant effects from soil type, tree species, or stand age ($p = 0.33$, 0.08, and 0.99, respectively, Fig. 3). RH varied from 154 to 290 $g\ C\ m^{-2}\ yr^{-1}$ across the 50 stands, whereas the autotrophic forest-floor respiration (RA_{ff}) ranged from 135 to 348 $g\ C\ m^{-2}\ yr^{-1}$. Neither of these R_{ff} components correlated significantly to soil type, tree species, or stand age ($p > 0.05$, Fig. 3, Supplementary Table S9). However, the individual RA_{ff} components were oppositely affected by stand age, with RA_u significantly decreasing ($p < 0.001$) from 109 ± 29 to $36 \pm 19\ g\ C\ m^{-2}\ yr^{-1}$ and RA_{tr} marginally increasing ($p = 0.058$) from 97 ± 39 to $191 \pm 103\ g\ C\ m^{-2}\ yr^{-1}$ from initiation to old-growth stands, respectively.

Across the 50 stands, the carbon-use efficiency of understory vegetation (CUE_u, NPP_u:GPP_u ratio) ranged from 0.50 to 0.71 (Supplementary Fig. S5), but was not affected by soil type, tree species, or stand age ($p > 0.05$). However, CUE_u exhibited a weak increase with increasing stand development (from 0.59 ± 0.05 in initiation to 0.67 ± 0.09 in old-growth stands, Fig. 5). The ratio of below- to aboveground net primary production of understory vegetation ($BNPP_u$:$ANPP_u$) varied from 0.45 to 2.01 (Supplementary Fig. S5) and was not affected by neither soil type, tree species nor stand age ($p > 0.05$, Fig. 5). Nonetheless, the ratio was on average somewhat higher in pine than in spruce stands (1.37 ± 0.73 and 1.05 ± 0.49, respectively) and slightly decreased with stand age (from 1.46 ± 0.59 to 0.93 ± 0.50 from young to mature stands). The ratio of autotrophic to heterotrophic forest-floor respiration fluxes (RA_{ff}:RH) ranged from 0.57 to 1.91 (Supplementary Fig. S5) without any significant effect from soil type, tree species, or stand age ($p > 0.05$),

although a somewhat increasing ratio was noted as stands aged (from 0.95 ± 0.39 in initiation to 1.33 ± 0.50 in mature stands, Fig. 5).

3.3. Key biotic and abiotic drivers of the spatial variability in forest-floor CO_2 fluxes

Our MLR analysis (Table 3) showed a moderate positive correlation between C_t and NE_{ff} (Adj. $R^2 = 0.39$), suggesting greater forest-floor net CO_2 emissions with increasing ecosystem carbon stock. GPP_u was strongly and negatively correlated to C_t (Adj. partial $R^2 = 0.72$), whereas it was weakly associated with C_u, soil C:N ratio, and Ta_{bc} (Adj. partial $R^2 = 0.05$, 0.02, and 0.01, respectively). NPP_u was strongly and negatively correlated to C_t (Adj. partial $R^2 = 0.60$), but only weakly to C_u (Adj. partial $R^2 = 0.06$). Meanwhile, $ANPP_u$ were mostly related to C_t through a negative relationship (Adj. $R^2 = 0.45$). In contrast, $BNPP_u$ showed a moderate positive correlation with C_u (Adj. partial $R^2 = 0.49$), but it was weakly correlated to stand age (Adj. partial $R^2 = 0.05$). Among the considered factors, no significant relationship was found for R_{ff}. However, RA_{ff} was weakly and negatively correlated with Ta_{bc} (Adj. $R^2 = 0.13$). The spatial variation of RA_u was strongly and negatively associated with C_t (Adj. partial $R^2 = 0.66$). However, adding Ta_{bc}, soil C:N ratio, and C_u, the total explanatory power for RA_u increased from 0.66 to 0.76. Furthermore, a weak negative correlation between C_t and RA_{tr} was also revealed (Adj. $R^2 = 0.21$). The best explaining factors of RH were Ts_{10} and soil C:N ratio (Adj. partial $R^2 = 0.07$ and 0.06, respectively), which showed weak positive and negative correlations with RH, respectively. Furthermore, the correlations between each of the studied forest-floor CO_2 fluxes and their primary drivers (i.e., C_t, C_u, Ta_{bc}, and Ts_{10}) were unaffected by soil type and tree species, except for NE_{ff}, RA_{ff},
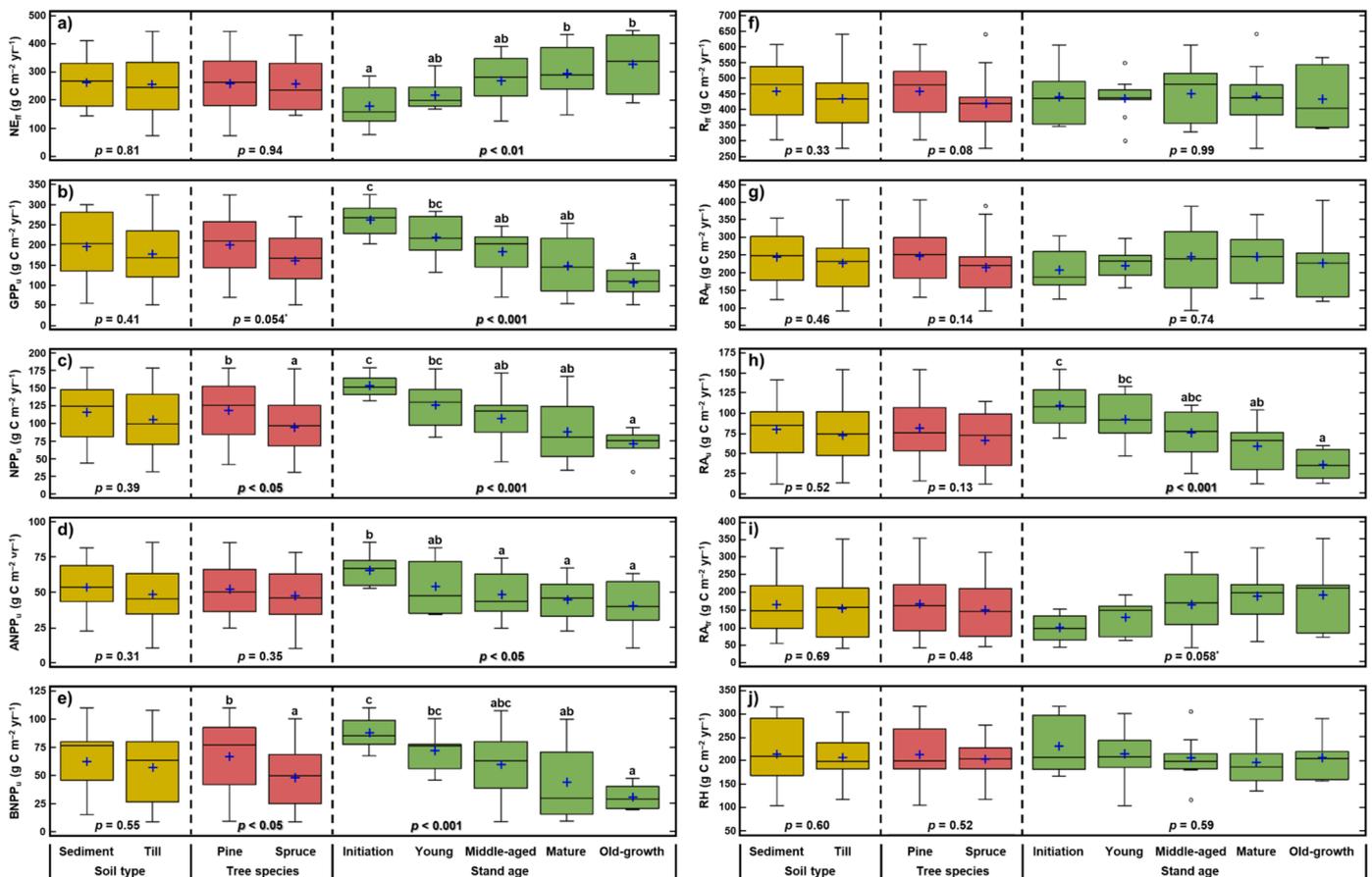
Fig. 3. Box plots representing the annual forest-floor CO_2 fluxes (see Fig. 1 for flux definitions; g C m^{-2} yr^{-1}) grouped according to key forest landscape attributes (i. e., soil type, tree species, and stand age). a) net forest-floor CO_2 exchange (NE$_{ff}$), b) gross primary production of understory vegetation (GPP$_u$), c) net primary production of understory vegetation (NPP$_u$), d) aboveground net primary production of understory vegetation (ANPP$_u$), e) belowground net primary production of understory vegetation (BNPP$_u$), f) total forest-floor respiration (R$_{ff}$), g) autotrophic forest-floor respiration (RA$_{ff}$), h) autotrophic respiration of understory vegetation (RA$_u$), i) autotrophic respiration of tree roots (RA$_{tr}$), and j) heterotrophic soil respiration (RH). Data based on 3-year (2016−2018) mean annual values. The boxes represent the 25th (bottom) and 75th (top) percentiles, the central line the median, and the cross the mean. Whiskers below and above the box denote data within 1.5 times of the interquartile range and outliers are given as individual points. Significant effects are marked in bold. Different superscript letters denote significant differences (Bonferroni test, $p < 0.05$) for each main effect. * denotes marginally significant p-values.
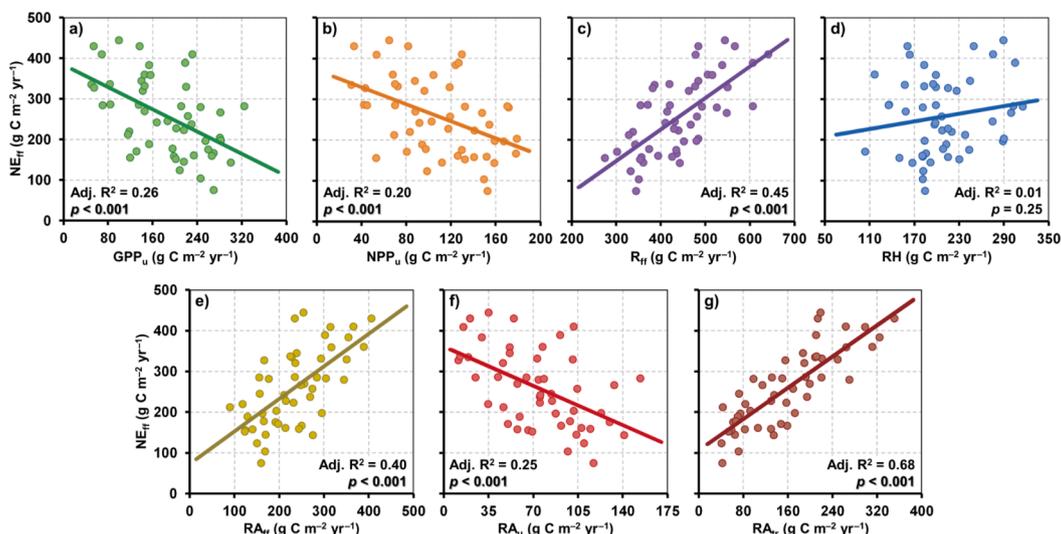

Fig. 4. Relationships of the net forest-floor CO_2 exchange (NE$_{ff}$) with a) gross primary production of understory vegetation (GPP$_u$), b) net primary production of understory vegetation (NPP$_u$), c) total forest-floor respiration (R$_{ff}$), d) heterotrophic soil respiration (RH), e) autotrophic forest-floor respiration (RA$_{ff}$), f) autotrophic respiration of understory vegetation (RA$_u$), and g) autotrophic respiration of tree roots (RA$_{tr}$) across the 50 stands. Dots and lines represent the 3-year (2016−2018) mean annual values and linear regression fit line, respectively. Adjusted coefficient of determination (Adj. R^2) and p-value are shown. $n = 50$ stands.
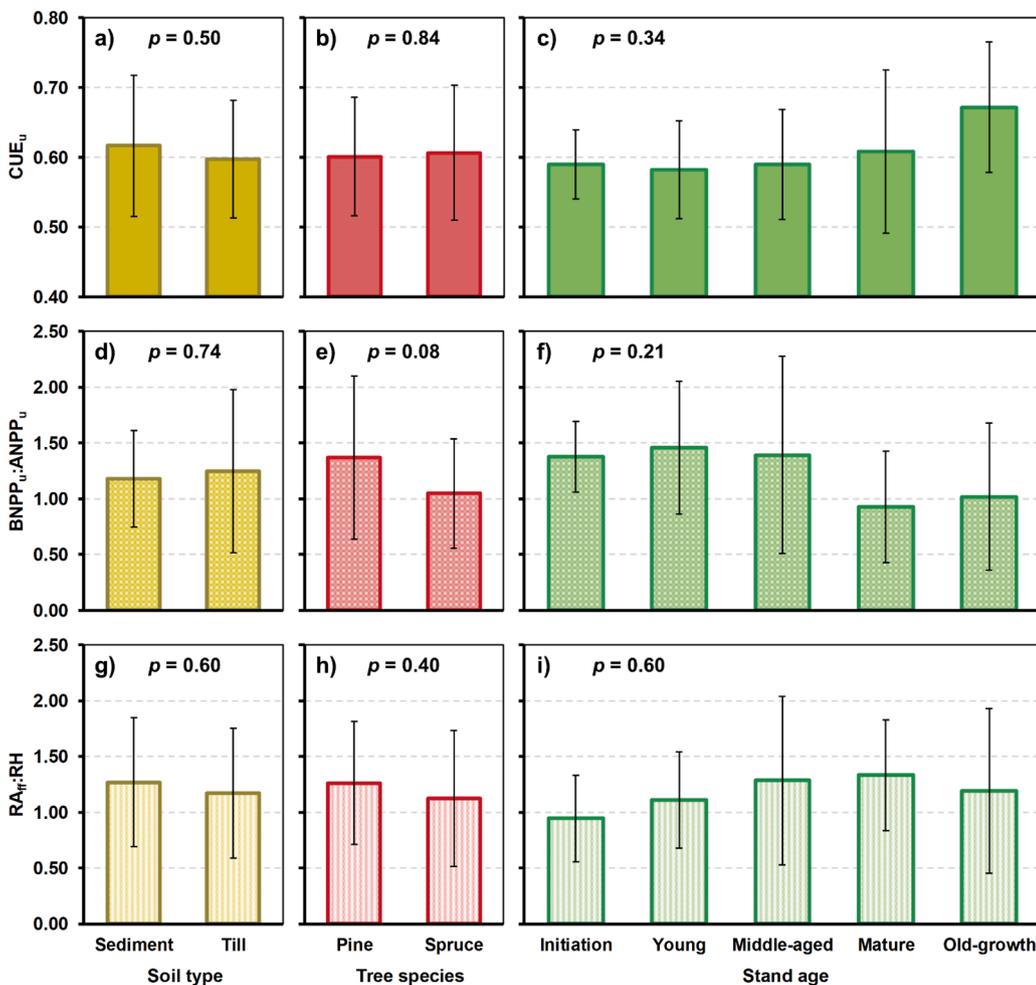
Fig. 5. Ratios between forest-floor CO_2 fluxes grouped according to key forest landscape attributes (i.e., soil type, tree species, and stand age). a–c) Net to gross primary production of understory vegetation (NPP_u:GPP_u, i.e., carbon use efficiency of understory vegetation, CUE_u), d–f) below- to aboveground net primary production of understory vegetation ($BNPP_u$:$ANPP_u$), and g–i) autotrophic forest-floor to heterotrophic soil respiration (RA_{ff}:RH). Values represent the 3-year (2016−2018) mean with standard deviation in whiskers. Non-significant differences were found ($p > 0.05$).

and RA_{tr}, which were higher in pine compared to spruce stands (Supplementary Figs. S6–S7).

4. Discussion

This study provides a detailed analysis of the landscape-scale variability in the net forest-floor CO_2 exchange (NE_{ff}) and its component fluxes and, thus, serves as a step towards a more process-based understanding of their magnitudes, relative contributions, and controlling factors. Such detailed knowledge is essential for evaluating the sensitivity of the boreal forest carbon balance to gradients in edaphic and structural attributes as well as forest management strategies and climate-forcing processes.

4.1. How do forest-floor CO_2 fluxes vary across a managed boreal forest landscape?

Our findings demonstrate that the forest-floor consistently acts as an annual net CO_2 source in all stand types within the boreal-forested landscape, however, with considerable variation noted in the source strength (149 to 399 g C m^{-2} yr^{-1}). The range in NE_{ff} observed within the studied landscape encompasses the majority of NE_{ff} estimates from previous forest site-level studies in the boreal region (e.g., Chi et al., 2021; Gaumont-Guay et al., 2009, 2014; Grant et al., 2001; Launiainen et al., 2005; Ťupek et al., 2008). However, it is noteworthy that NE_{ff} estimates exceeding 1000 g C m^{-2} yr^{-1} have been occasionally reported (Morén and Lindroth, 2000; Widén, 2002). To date, it has remained unclear to what extent this variation in the net forest-floor CO_2 exchange

was driven by geographical and/or climatic gradients or intrinsic landscape properties. Here, we reveal the spatial variability in NE_{ff} and its underlying component fluxes within a single boreal catchment, removing potentially confounding effects from trans-regional gradients.

The range of the gross primary production of understory vegetation (GPP_u) within our studied catchment (77–275 g C m^{-2} yr^{-1}) is within the maximum–minimum span of 30–350 g C m^{-2} yr^{-1} reported from single-site studies in boreal forests (e.g., Bergeron et al., 2009; Chi et al., 2021; Gaumont-Guay et al., 2014; Kulmala et al., 2011, 2019; Palmroth et al., 2019; Ťupek et al., 2008). The similar GPP_u span, when comparing that of the studied landscape with the one reported across various boreal sites, suggests that variations in understory photosynthetic rates within the boreal region are driven primarily by landscape characteristics rather than by geographical/climatic gradients. We also note that the average GPP_u of 183 $\pm$ 72 g C m^{-2} yr^{-1} across the 50 stands indicates that understory photosynthesis represents a substantial contribution to landscape-scale gross primary production, which in the same catchment was previously estimated at 805 $\pm$ 28 g C m^{-2} yr^{-1} based on tall-tower eddy covariance measurements (Chi et al., 2019).

Our findings further reveal that total forest-floor respiration (R_{ff}) is more important than GPP_u in controlling the landscape-scale variation in NE_{ff} (Fig. 4). Therefore, acquiring comprehensive data on forest-floor respiration sources (incorporating soil, tree roots, and understory vegetation) will be particularly important for improving our understanding of the landscape-scale net forest-floor CO_2 budget. Specifically, the range of R_{ff} across the studied landscape (340–549 g C m^{-2} yr^{-1}) is within the lower half of the minimum–maximum range of 350–900 g C m^{-2} yr^{-1} reported by previous boreal site-level studies (e.g., Chi et al.,

Table 3

Coefficients (b_0, b_1, b_2, b_3, b_4) and their standard errors (SE), adjusted coefficients of partial and total determination (Adj. partial R^2 and Adj. R^2, respectively), standard error of estimate (SEE), and *p*-value of multiple linear regressions determined among annual forest-floor CO_2 fluxes (g C m^{-2} yr^{-1}) and biotic and/or abiotic factors. See Fig. 1 for flux definitions. Adj. partial R^2 values are presented following the order of the independent variables (IV) in the regression. Data based on 3-year (2016−2018) mean annual values. Non-significant regressions are denoted as *ns*. n = 50 stands.

Regression	Coefficients					SE Coefficients					Adj. partial R^2				Adj. R^2	SEE	*p*
	b_0	b_1	b_2	b_3	b_4	b_0	b_1	b_2	b_3	b_4	IV 1	IV 2	IV 3	IV 4			
1	$NE_{ff} = b_0 + b_1 \times C_t$																
1	164	1.46	–	–	–	20	0.26	–	–	–	0.39	–	–	–	0.39	74.1	< 0.001
2	$GPP_u = b_0 + b_1 \times C_t + b_2 \times C_u + b_3 \times C{:}N + b_4 \times Ta_{bc}$																
2	333	−1.17	23.27	−2.29	−18.98	56	0.19	5.69	1.00	9.17	0.72	0.05	0.02	0.01	0.80	32.0	< 0.001
3	$NPP_u = b_0 + b_1 \times C_t + b_2 \times C_u$																
3	95	−0.46	12.91	–	–	22	0.13	4.15	–	–	0.60	0.06	–	–	0.66	24.1	< 0.001
4	$ANPP_u = b_0 + b_1 \times C_t$																
4	69	−0.29	–	–	–	3	0.05	–	–	–	0.45	–	–	–	0.45	13.1	< 0.001
5	$BNPP_u = b_0 + b_1 \times C_u + b_2 \times Age$																
5	33	12.22	−0.21	–	–	13	2.56	0.08	–	–	0.49	0.05	–	–	0.54	20.2	< 0.001
6	R_{ff}																
6	–	–	–	–	–	–	–	–	–	–	–	–	–	–	–	–	*ns*
7	$RA_{ff} = b_0 + b_1 \times Ta_{bc}$																
7	418	−48.27	–	–	–	65	16.69	–	–	–	0.13	–	–	–	0.13	71.1	< 0.01
8	$RA_u = b_0 + b_1 \times C_t + b_2 \times Ta_{bc} + b_3 \times C{:}N + b_4 \times C_u$																
8	199	−0.68	−14.92	−1.57	9.15	31	0.10	5.00	0.55	3.11	0.66	0.04	0.04	0.02	0.76	17.5	< 0.001
9	$RA_{tr} = b_0 + b_1 \times C_t$																
9	97	0.94	–	–	–	19	0.25	–	–	–	0.21	–	–	–	0.21	72.5	< 0.001
10	$RH = b_0 + b_1 \times Ts_{10} + b_2 \times C{:}N$																
10	239	18.89	−2.96	–	–	47	6.65	1.40	–	–	0.07	0.06	–	–	0.13	47.0	< 0.05

Independent variables included in the regressions are basal area-weighted mean stand age (Age, yr), total tree biomass carbon stock (C_t, Mg C ha^{-1}), total understory biomass carbon stock (C_u, Mg C ha^{-1}), below-canopy air temperature (Ta_{bc}, °C), soil temperature at 10 cm depth (Ts_{10}, °C), and average soil carbon-nitrogen ratio up to 20 cm depth (C:N, dimensionless).

2021; Gaumont-Guay et al., 2009, 2014; Grant et al., 2001; Launiainen et al., 2005; Ryhti et al., 2021; Ťupek et al., 2008). Thus, in contrast to GPP_u, geographical and/or climatic conditions (e.g., seasonal temperature dynamics) might override and/or further modify intrinsic landscape features in regulating the spatial heterogeneity in R_{ff} within the boreal biome. Our results also suggest that the large range in the relative contribution of autotrophic and heterotrophic respiration (RA_{ff} and RH, respectively) to R_{ff} (0.57–1.91) is primarily due to the variations in the RA_{ff} components, whereas RH remains relatively stable across the 50 stands. This further implies that the physiological response of RA_{ff} to perturbations from forest management and climate change is an important driver for associated changes in the forest-floor CO_2 emissions. Given the potential bias in our RH and RA_{ff} estimates, however, future efforts should focus on refining these estimates and related patterns in the boreal landscape. The average R_{ff} of 440 ± 84 g C m^{-2} yr^{-1} across the 50 stands also indicates a substantial contribution to landscape-scale respiration, which was previously estimated at 710 ± 25 g C m^{-2} yr^{-1} for the same catchment (Chi et al., 2019). Thus, given the large range and contribution of R_{ff} within and its potential vulnerability to climate warming (Bond-Lamberty and Thomson, 2010), the forest-floor plays a pivotal role in the response of the carbon balance of boreal forest landscapes to global change impacts.

4.2. What is the sensitivity of the forest-floor CO_2 fluxes to key landscape attributes?

Soil type, tree species, and stand age are widely acknowledged key landscape attributes modulating understory productivity and soil biogeochemistry (Barbier et al., 2008; Chen and Shrestha, 2012; Hedwall et al., 2013; Kumar et al., 2018a; Laganière et al., 2012; Marek and Richardson, 2020). The lack of soil type and tree species effects on NE_{ff} observed in this study appears, thus, surprising at first. However, we show that counterbalancing dynamics in understory photosynthesis and total forest-floor respiration may explain the absence of soil and tree effects on the net forest-floor CO_2 exchange. Meanwhile, NE_{ff} is strongly affected by stand age in response to decreasing GPP_u, with R_{ff} remaining fairly stable among age classes (Fig. 3). Therefore, we demonstrate that stand age is a strong regulator of the net CO_2 emissions at the boreal forest-floor interface, emphasizing that perturbations of forest age structure (e.g., by management or natural disturbance) may largely alter forest-floor CO_2 exchange dynamics.

Consistent with previous works (Kulmala et al., 2011; Landuyt et al., 2019; Petersson et al., 2019), our study also demonstrates the influence of structural attributes on modulating understory growth conditions and production rates across the landscape. Specifically, increased light availability and warmer air temperature at the forest-floor promoted higher GPP_u and NPP_u in pine compared to spruce stands (Supplementary Fig. S8). It is also worth noting that production rates show maximum values during the early stages of stand development, which suggests that understory establishes rapidly following forest clear cutting, likely due to increased resource availability such as light, water, and soil nutrients (Barbier et al., 2008; Kumar et al., 2018b). Thereafter, both GPP_u and NPP_u decrease with stand development in response to a simultaneous reduction in light availability and temperature (Table 1), understory biomass (Table 2), and photosynthetic activity rates (Supplementary Fig. S9), likely in combination with an increase in interspecific nutrient/water competition between tree and understory roots (Landuyt et al., 2019; Nilsson and Wardle, 2005).

The large variability in the understory carbon use efficiency (CUE_u, NPP_u:GPP_u ratio; range 0.50–0.71) was similar to that previously reported for forest ecosystems in which the forest-floor is dominated by shrub and herbaceous species (range 0.40–0.70, Zhang et al., 2009). However, it is important to note that a weak tendency to higher CUE_u values was observed with increasing stand age (Fig. 5), which might be due to the increasing contribution from mosses, which have a higher carbon use efficiency rates than other plant functional types (Street

et al., 2013). Additionally, the observed increase in nitrogen availability (i.e., lower C:N ratio) and decrease in below-canopy temperature during stand development may further explain the age-related increase in CUE_u, which is in line with previous findings (Bradford and Crowther, 2013; Vicca et al., 2012).

Our study also sheds light on the largely understudied patterns of NPP_u allocation. Specifically, our observation that larger amount of biomass is allocated below- than aboveground may reflect an adaptation of the shallow-rooted understory species in order to allow nutrient and water supply in the resource-limited understory environments of boreal forests. Interestingly, we also found that the belowground contribution to NPP_u is lower in spruce than in pine stands and it also decreases with stand development (Fig. 5), suggesting that understory responds to reduced light availability by increasing carbon allocation toward aboveground growth (Kumordzi et al., 2016; Poorter et al., 2012). In addition, changes in the dominance of plant functional types (Supplementary Fig. S10) and their inherent differences in biomass allocation patterns may also be involved in the increasing aboveground photosynthate carbon allocation as stands age. It is however noteworthy that despite our extensive efforts, methodological assumptions required to estimate NPP_u over the 3-year study period still led to considerable uncertainty in the interpretation of understory production and allocation results. Thus, improving our knowledge on NPP_u dynamics remains a key research challenge.

This study further demonstrates that neither edaphic nor structural landscape attributes affect R_{ff} (Fig. 3). This fact could be due to counteracting effects of the various controls across the complex landscape. For instance, we found that sediment soils and pine stands show warmer forest-floor conditions (Table 1) and higher understory biomass (Table 2), but R_{ff} rates show no significant difference with those of till soils and spruce stands because R_{ff} could be positively affected in the latter by their higher levels of SOC (Table 2) and tree root biomass (Supplementary Fig. S11). It is also noteworthy that the lack of effect of stand age on the underlying components of R_{ff} (see discussed below) prevents the emergence of a clear pattern of R_{ff} along the age gradient.

The absence of substantial variations in RH during stand development (Fig. 3) is in contrast with the common understanding that this flux, after an initial pulse following clear cutting, steadily increases with stand age (Harmon et al., 2011; Saiz et al., 2006). One possible explanation for the lack of high RH in our recent clear-felled stands could be that relative to temperate regions (Pregitzer and Euskirchen, 2004), lower soil nutrient availability and colder temperature may limit microbial decomposition rates during the early stages of stand development in the boreal region. Thereafter, the offset between decreasing soil temperature and increasing amounts of SOC might explain the fairly invariant level of RH observed during stand development.

Similar to RH, we also observed a lack of stand age effect on RA_{ff}, which was likely because the increase in the autotrophic respiration of tree roots (RA_{tr}) was balanced by the decrease in that of understory vegetation (RA_u) during stand development. These parallel dynamics are well-reflected by the wide range in the ratio of RA_{tr}:RA_u, which increased from 0.9 in initiation stands to 7.3 in old-growth stands, demonstrating a considerable age-related shift in the main control of RA_{ff} across the landscape. Overall, this study highlights the need for a detailed understanding of the controls and relative contributions from the separate autotrophic forest-floor respiration components in order to improve our ability to predict ecosystem carbon balance responses to climate change.

4.3. Which key biotic and abiotic factors modulate the spatial variability of forest-floor CO_2 fluxes across a managed boreal forest landscape?

In a next step, we further assessed in more detail which specific biotic and abiotic factors drive the spatial variability of forest-floor CO_2 fluxes. Our MLR analysis reveals that tree biomass (C_t) largely shapes the landscape-scale patterns of NE_{ff} and most of its underlying component

fluxes (Table 3). This result is supported by the significant control that overstory biomass exerts on remaining ecosystem biomass components as well as resource availability and growing conditions at the forest-floor (Supplementary Fig. 12). Our findings therefore demonstrate that changes in the overstory tree dynamics in response to forest management and/or global change might significantly modulate the magnitudes and spatial variation of the forest-floor CO_2 fluxes in boreal forests.

The observed positive correlation between NE_{ff} and C_t might be mainly caused by changes in RA_{tr} (Fig. 4). Not surprisingly, RA_{tr} tends to increase with tree biomass (Table 3), which is largely attributable to concurrent increases in tree root biomass and respiration. It should also be noted that RA_{tr} (and NE_{ff}) differed between pine and spruce stands (Supplementary Fig. S7). This tree species effect may arise from the lower RA_{tr} rates observed in spruce stands at maximum C_t values, which in turn might be directly associated with the coincident decrease in fine-root biomass (Supplementary Fig. 13). While it is known that fine root biomass gradually declines in maturing stands (Yuan and Chen, 2010), the reason for the faster decrease in spruce than in pine stands observed in our study remains elusive.

The negative correlation of understory production to tree biomass might be explained by overstory effects on understory light environment and growing conditions (Barbier et al., 2008; Landuyt et al., 2019). Previous studies suggested that ignoring understory dynamics may result in biased estimates of forest productivity (Kolari et al., 2006; Nilsson and Wardle, 2005). The tight relationships between C_t and both GPP_u and NPP_u observed in our study further underline the need for mapping these largely understudied CO_2 fluxes in boreal forest ecosystems.

Forest microclimate, specifically below-canopy air temperature (Ta_{bc}), appears to control the RA_{ff} rates across the studied landscape. However, the weak negative correlation between RA_{ff} and Ta_{bc} may be partially due to confounding effects on the RA_{tr} component attributed to the negative covariance between Ta_{bc} and C_t (Supplementary Fig. S12). In addition, it is worth noting that warmer conditions in pine than in spruce stands resulted in a greater RA_{ff} (Supplementary Fig. S7), in line with the well-known temperature dependency of autotrophic respiration (Atkin and Tjoelker, 2003). In contrast to RA_{tr}, RA_u decreased with increasing tree biomass, which was primarily due to the concurrent trends of decreasing understory biomass and increasing CUE_u. Thus, our study highlights the complexity of autotrophic forest-floor respiration and the need for more empirical evidence to resolve existing uncertainties in this carbon cycle component.

Our results further suggest that overstory effects on soil temperature (Ts_{10}) may play an important role in regulating landscape-scale soil decomposition dynamics (Table 3). Interestingly, the higher apparent temperature sensitivity of RH in young stands (i.e., Q_{10} values, see Supplementary Fig. S15 in Supplementary materials, Section 16) indicates that climate-driven temperature increases (Bond-Lamberty et al., 2018) might enhance RH particularly during the initial stand development. Altogether, our results therefore suggest that soil carbon-climate feedbacks might be highly variable at the landscape-scale, which must be considered when assessing the response of the boreal forest carbon balance to climate change.

5. Conclusions

Our study provides evidence for the large spatial variability in forest-floor CO_2 fluxes across the boreal landscape in response to multiple processes and their different controls. This highlights the need for a detailed understanding of these various processes underlying the net forest-floor CO_2 exchange (NE_{ff}) to improve process-based models with the aim to more accurately predict responses of the boreal forest carbon cycle to external forcings. Our study also reveals that among the key landscape attributes, stand age acts as the dominant control on modulating most forest-floor CO_2 fluxes. In comparison, tree species only affects understory production and soil type has no effect on any of the NE_{ff}

component fluxes. Based on our results, we further conclude that among the investigated abiotic and biotic factors, tree biomass is the major driver of the landscape-scale variations of CO_2 fluxes, likely attributable to modulating effects on resource availability and growing conditions at the forest-floor interface. This further implies that consequences from changes in climatic conditions and forest management strategies for forest-floor CO_2 dynamics are tightly coupled to the responses of tree canopy structure and biomass allocation.

Author contributions

MP, MBN, and HL conceived the study; MP, EMG, JESF, and JW planned and conducted the data collection; EMG, MP, and MBN interpreted the data; EMG wrote the manuscript with input from MP, MBN, HL, TL, JESF, and JW.

Declaration of Competing Interest

The authors declare that they have no known competing financial interests or personal relationships that could have appeared to influence the work reported in this paper.

Data Availability

The data sets that support the findings of this study are openly available in the Zenodo digital repository at https://doi.org/10.5281/zenodo.5730154.

Code Availability

This manuscript does not include code.

Supplementary materials

Supplementary material associated with this article can be found, in the online version, at doi:10.1016/j.agrformet.2022.108916.

References

Aguinaga-Gil, I., 2018. MSc Thesis Thesis. Wageningen University and Research (WUR), p. 37.

Atkin, O.K., Tjoelker, M.G., 2003. Thermal acclimation and the dynamic response of plant respiration to temperature. Trends Plant Sci. 8 (7), 343–351. https://doi.org/10.1016/S1360-1385(03)00136-5.

Baldocchi, D.D., 2014. Measuring fluxes of trace gases and energy between ecosystems and the atmosphere – the state and future of the eddy covariance method. Glob. Change Biol. 20 (12), 3600–3609. https://doi.org/10.1111/gcb.12649.

Barbier, S., Gosselin, F., Balandier, P., 2008. Influence of tree species on understory vegetation diversity and mechanisms involved—A critical review for temperate and boreal forests. Forest Ecol. Manag. 254 (1), 1–15. https://doi.org/10.1016/j.foreco.2007.09.038.

Beer, C., Reichstein, M., Tomelleri, E., Ciais, P., Jung, M., Carvalhais, N., Rödenbeck, C., Arain, M.A., Baldocchi, D., Bonan, G.B., Bondeau, A., Cescatti, A., Lasslop, G., Lindroth, A., Lomas, M., Luyssaert, S., Margolis, H., Oleson, K.W., Roupsard, O., Veenendaal, E., Viovy, N., Williams, C., Woodward, F.I., Papale, D., 2010. Terrestrial gross carbon dioxide uptake: global distribution and covariation with climate. Science 329 (5993), 834–838. https://doi.org/10.1126/science.1184984.

Bergeron, O., Margolis, H.A., Coursolle, C., 2009. Forest floor carbon exchange of a boreal black spruce forest in eastern North America. Biogeosciences 6 (9), 1849–1864. https://doi.org/10.5194/bg-6-1849-2009.

Bond-Lamberty, B., Bailey, V.L., Chen, M., Gough, C.M., Vargas, R., 2018. Globally rising soil heterotrophic respiration over recent decades. Nature 560 (7716), 80–83. https://doi.org/10.1038/s41586-018-0358-x.

Bond-Lamberty, B., Bronson, D., Bladyka, E., Gower, S.T., 2011. A comparison of trenched plot techniques for partitioning soil respiration. Soil Biol. Biochem. 43 (10), 2108–2114. https://doi.org/10.1016/j.soilbio.2011.06.011.

Bond-Lamberty, B., Thomson, A., 2010. Temperature-associated increases in the global soil respiration record. Nature 464 (7288), 579–582. https://doi.org/10.1038/nature08930.

Bond-Lamberty, B., Wang, C., Gower, S.T., 2004. A global relationship between the heterotrophic and autotrophic components of soil respiration? Glob. Change Biol. 10 (10), 1756–1766. https://doi.org/10.1111/j.1365-2486.2004.00816.x.

Bradford, M.A., Crowther, T.W., 2013. Carbon use efficiency and storage in terrestrial ecosystems. New Phytol. 199 (1), 7–9. https://doi.org/10.1111/nph.12334.

Campioli, M., Malhi, Y., Vicca, S., Luyssaert, S., Papale, D., Peñuelas, J., Reichstein, M., Migliavacca, M., Arain, M.A., Janssens, I.A., 2016. Evaluating the convergence between eddy-covariance and biometric methods for assessing carbon budgets of forests. Nat. Commun. 7 (1), 13717. https://doi.org/10.1038/ncomms13717.

Chapin, F.S., Woodwell, G.M., Randerson, J.T., Rastetter, E.B., Lovett, G.M., Baldocchi, D.D., Clark, D.A., Harmon, M.E., Schimel, D.S., Valentini, R., Wirth, C., Aber, J.D., Cole, J.J., Goulden, M.L., Harden, J.W., Heimann, M., Howarth, R.W., Matson, P.A., McGuire, A.D., Melillo, J.M., Mooney, H.A., Neff, J.C., Houghton, R.A., Pace, M.L., Ryan, M.G., Running, S.W., Sala, O.E., Schlesinger, W.H., Schulze, E.D., 2006. Reconciling carbon-cycle concepts, terminology, and methods. Ecosystems 9 (7), 1041–1050. https://doi.org/10.1007/s10021-005-0105-7.

Chen, H.Y.H., Shrestha, B.M., 2012. Stand age, fire and clearcutting affect soil organic carbon and aggregation of mineral soils in boreal forests. Soil Biol. Biochem. 50, 149–157. https://doi.org/10.1016/j.soilbio.2012.03.014.

Chi, J., Nilsson, M.B., Kljun, N., Wallerman, J., Fransson, J.E.S., Laudon, H., Lundmark, T., Peichl, M., 2019. The carbon balance of a managed boreal landscape measured from a tall tower in northern Sweden. Agr. Forest Meteorol. 274, 29–41. https://doi.org/10.1016/j.agrformet.2019.04.010.

Chi, J., Zhao, P., Klosterhalfen, A., Jocher, G., Kljun, N., Nilsson, M.B., Peichl, M., 2021. Forest floor fluxes drive differences in the carbon balance of contrasting boreal forest stands. Agr. Forest Meteorol. 306, 108454 https://doi.org/10.1016/j.agrformet.2021.108454.

Collatz, G.J., Ribas-Carbo, M., Berry, J.A., 1992. Coupled photosynthesis-stomatal conductance model for leaves of C₄ plants. Funct. Plant Biol. 19 (5), 519–538. https://doi.org/10.1071/PP9920519.

Curiel Yuste, J., Baldocchi, D.D., Gershenson, A., Goldstein, A., Misson, L., Wong, S., 2007. Microbial soil respiration and its dependency on carbon inputs, soil temperature and moisture. Glob. Change Biol. 13 (9), 2018–2035. https://doi.org/10.1111/j.1365-2486.2007.01415.x.

Davidson, E.A., Janssens, I.A., 2006. Temperature sensitivity of soil carbon decomposition and feedbacks to climate change. Nature 440 (7081), 165–173. https://doi.org/10.1038/nature04514.

Dixon, R.K., Solomon, A.M., Brown, S., Houghton, R.A., Trexier, M.C., Wisniewski, J., 1994. Carbon pools and flux of global forest ecosystems. Science 263 (5144), 185–190. https://doi.org/10.1126/science.263.5144.185.

Gaumont-Guay, D., Black, T.A., Barr, A.G., Griffis, T.J., Jassal, R.S., Krishnan, P., Grant, N., Nesic, Z., 2014. Eight years of forest-floor CO₂ exchange in a boreal black spruce forest: spatial integration and long-term temporal trends. Agr. Forest Meteorol. 184, 25–35. https://doi.org/10.1016/j.agrformet.2013.08.010.

Gaumont-Guay, D., Black, T.A., McCaughey, H., Barr, A.G., Krishnan, P., Jassal, R.S., Nesic, Z., 2009. Soil CO₂ efflux in contrasting boreal deciduous and coniferous stands and its contribution to the ecosystem carbon balance. Glob. Change Biol. 15 (5), 1302–1319. https://doi.org/10.1111/j.1365-2486.2008.01830.x.

Goulden, M.L., McMillan, A.M.S., Winston, G.C., Rocha, A.V., Manies, K.L., Harden, J.W., Bond-Lamberty, B.P., 2011. Patterns of NPP, GPP, respiration, and NEP during boreal forest succession. Glob. Change Biol. 17 (2), 855–871. https://doi.org/10.1111/j.1365-2486.2010.02274.x.

Grant, R.F., Goulden, M.L., Wofsy, S.C., Berry, J.A., 2001. Carbon and energy exchange by a black spruce-moss ecosystem under changing climate: testing the mathematical model ecosys with data from the BOREAS experiment. J. Geophys. Res.:Atmos. 106 (D24), 33605–33621. https://doi.org/10.1029/2001JD900064.

Harmon, M.E., Bond-Lamberty, B., Tang, J., Vargas, R., 2011. Heterotrophic respiration in disturbed forests: a review with examples from North America. J. Geophys. Res.: Biogeo. 116 (G4) https://doi.org/10.1029/2010JG001495.

Hedwall, P.-O., Brunet, J., Nordin, A., Bergh, J., 2013. Changes in the abundance of keystone forest floor species in response to changes of forest structure. J. Veg. Sci. 24 (2), 296–306. https://doi.org/10.1111/j.1654-1103.2012.01457.x.

Hiltbrunner, D., Zimmermann, S., Karbin, S., Hagedorn, F., Niklaus, P.A., 2012. Increasing soil methane sink along a 120-year afforestation chronosequence is driven by soil moisture. Glob. Change Biol. 18 (12), 3664–3671. https://doi.org/10.1111/j.1365-2486.2012.02798.x.

Högberg, P., Bhupinderpal, S., Löfvenius, M.O., Nordgren, A., 2009. Partitioning of soil respiration into its autotrophic and heterotrophic components by means of tree-girdling in old boreal spruce forest. Forest Ecol. Manag. 257 (8), 1764–1767. https://doi.org/10.1016/j.foreco.2009.01.036.

Holmström, E., Goude, M., Nilsson, O., Nordin, A., Lundmark, T., Nilsson, U., 2018. Productivity of Scots pine and Norway spruce in central Sweden and competitive release in mixtures of the two species. Forest Ecol. Manag. 429, 287–293. https://doi.org/10.1016/j.foreco.2018.07.008.

Hume, A., Chen, H.Y.H., Taylor, A.R., Kayahara, G.J., Man, R., 2016. Soil C:N:P dynamics during secondary succession following fire in the boreal forest of central Canada. Forest Ecol. Manag. 369, 1–9. https://doi.org/10.1016/j.foreco.2016.03.033.

Hursh, A., Ballantyne, A., Cooper, L., Maneta, M., Kimball, J., Watts, J., 2017. The sensitivity of soil respiration to soil temperature, moisture, and carbon supply at the global scale. Glob. Change Biol. 23 (5), 2090–2103. https://doi.org/10.1111/gcb.13489.

Ikawa, H., Nakai, T., Busey, R.C., Kim, Y., Kobayashi, H., Nagai, S., Ueyama, M., Saito, K., Nagano, H., Suzuki, R., Hinzman, L., 2015. Understory CO₂, sensible heat, and latent heat fluxes in a black spruce forest in interior Alaska. Agr. Forest Meteorol. 214–215. https://doi.org/10.1016/j.agrformet.2015.08.247, 80-90.

Järveoja, J., Peichl, M., Maddison, M., Teemusk, A., Mander, Ü., 2016. Full carbon and greenhouse gas balances of fertilized and nonfertilized reed canary grass cultivations on an abandoned peat extraction area in a dry year. GCB Bioenergy 8 (5), 952–968. https://doi.org/10.1111/gcbb.12308.

Jocher, G., Ottosson Löfvenius, M., De Simon, G., Hörnlund, T., Linder, S., Lundmark, T., Marshall, J., Nilsson, M.B., Näsholm, T., Tarvainen, L., Öquist, M., Peichl, M., 2017. Apparent winter CO₂ uptake by a boreal forest due to decoupling. Agr. Forest Meteorol. 232, 23–34. https://doi.org/10.1016/j.agrformet.2016.08.002.

Kolari, P., Pumpanen, J., Kulmala, L., Ilvesniemi, H., Nikinmaa, E., Grönholm, T., Hari, P., 2006. Forest floor vegetation plays an important role in photosynthetic production of boreal forests. Forest Ecol. Manag. 221 (1), 241–248. https://doi.org/10.1016/j.foreco.2005.10.021.

Kulmala, L., Pumpanen, J., Kolari, P., Dengel, S., Berninger, F., Köster, K., Matkala, L., Vanhatalo, A., Vesala, T., Bäck, J., 2019. Inter- and intra-annual dynamics of photosynthesis differ between forest floor vegetation and tree canopy in a subarctic Scots pine stand. Agr. Forest Meteorol. 271, 1–11. https://doi.org/10.1016/j.agrformet.2019.02.029.

Kulmala, L., Pumpanen, J., Kolari, P., Muukkonen, P., Hari, P., Vesala, T., 2011. Photosynthetic production of ground vegetation in different-aged Scots pine (*Pinus sylvestris*) forests. Can. J. For. Res. 41 (10), 2020–2030. https://doi.org/10.1139/x11-121.

Kulmala, L., Pumpanen, J., Vesala, T., Hari, P., 2009. Photosynthesis of boreal ground vegetation after a forest clear-cut. Biogeosciences 6 (11), 2495–2507. https://doi.org/10.5194/bg-6-2495-2009.

Kumar, P., Chen, H.Y.H., Searle, E.B., Shahi, C., 2018a. Dynamics of understorey biomass, production and turnover associated with long-term overstorey succession in boreal forest of Canada. Forest Ecol. Manag. 427, 152–161. https://doi.org/10.1016/j.foreco.2018.05.066.

Kumar, P., Chen, H.Y.H., Thomas, S.C., Shahi, C., 2018b. Linking resource availability and heterogeneity to understorey species diversity through succession in boreal forest of Canada. J. Ecol. 106 (3), 1266–1276. https://doi.org/10.1111/1365-2745.12861.

Kumordzi, B.B., Gundale, M.J., Nilsson, M.-C., Wardle, D.A., 2016. Shifts in aboveground biomass allocation patterns of dominant shrub species across a strong environmental gradient. PLoS ONE 11 (6), e0157136. https://doi.org/10.1371/journal.pone.0157136.

Kuuluvainen, T., Gauthier, S., 2018. Young and old forest in the boreal: critical stages of ecosystem dynamics and management under global change. For. Ecosyst. 5 (1), 26. https://doi.org/10.1186/s40663-018-0142-2.

Laganière, J., Paré, D., Bergeron, Y., Chen, H.Y.H., 2012. The effect of boreal forest composition on soil respiration is mediated through variations in soil temperature and C quality. Soil Biol. Biochem. 53, 18–27. https://doi.org/10.1016/j.soilbio.2012.04.024.

Landuyt, D., De Lombaerde, E., Perring, M.P., Hertzog, L.R., Ampoorter, E., Maes, S.L., De Frenne, P., Ma, S., Proesmans, W., Blondeel, H., Sercu, B.K., Wang, B., Wasof, S., Verheyen, K., 2019. The functional role of temperate forest understorey vegetation in a changing world. Glob. Change Biol. 25 (11), 3625–3641. https://doi.org/10.1111/gcb.14756.

Laudon, H., Hasselquist, E.M., Peichl, M., Lindgren, K., Sponseller, R., Lidman, F., Kuglerová, L., Hasselquist, N.J., Bishop, K., Nilsson, M.B., Ågren, A.M., 2021. Northern landscapes in transition: evidence, approach and ways forward using the Krycklan Catchment Study. Hydrol. Process. 35 (4), e14170. https://doi.org/10.1002/hyp.14170.

Launiainen, S., Rinne, J., Pumpanen, J., Kulmala, L., Kolari, P., Keronen, P., Siivola, E., Pohja, T., Hari, P., Vesala, T., 2005. Eddy covariance measurements of CO₂ and sensible and latent heat fluxes during a full year in a boreal pine forest trunk-space. Boreal Environ. Res. 10 (6), 569–588.

Lloyd, J., Taylor, J.A., 1994. On the temperature dependence of soil respiration. Funct. Ecol. 8, 315–323. https://doi.org/10.2307/2389824.

Luyssaert, S., Inglima, I., Jung, M., Richardson, A.D., Reichstein, M., Papale, D., Piao, S. L., Schulze, E.-D., Wingate, L., Matteucci, G., Aragao, L., Aubinet, M., Beer, C., Bernhofer, C., Black, K.G., Bonal, D., Bonnefond, J.-M., Chambers, J., Ciais, P., Cook, B., Davis, K.J., Dolman, A.J., Gielen, B., Goulden, M., Grace, J., Granier, A., Grelle, A., Griffis, T., Grünwald, T., Guidolotti, G., Hanson, P.J., Harding, R., Hollinger, D.Y., Hutyra, L.R., Kolari, P., Kruijt, B., Kutsch, W., Lagergren, F., Laurila, T., Law, B.E., Le Maire, G., Lindroth, A., Loustau, D., Malhi, Y., Mateus, J., Migliavacca, M., Misson, L., Montagnani, L., Moncrieff, J., Moors, E., Munger, J.W., Nikinmaa, E., Ollinger, S.V., Pita, G., Rebmann, C., Roupsard, O., Saigusa, N., Sanz, M.J., Seufert, G., Sierra, C., Smith, M.-L., Tang, J., Valentini, R., Vesala, T., Janssens, I.A., 2007. CO2 balance of boreal, temperate, and tropical forests derived from a global database. Glob. Change Biol. 13 (12), 2509–2537. https://doi.org/10.1111/j.1365-2486.2007.01439.x.

Mäkinen, H., Hynynen, J., Siitonen, J., Sievänen, R., 2006. Predicting the decomposition of Scots pine, Norway spruce, and Birch stems in Finland. Ecol. Appl. 16 (5),

1865–1879. https://doi.org/10.1890/1051-0761, 2006016[1865:PTDOSP]2.0.CO; 2.

Makita, N., Pumpanen, J., Köster, K., Berninger, F., 2016. Changes in very fine root respiration and morphology with time since last fire in a boreal forest. Plant Soil 402 (1), 303–316. https://doi.org/10.1007/s11104-016-2801-9.

Marek, R.S., Richardson, J.B., 2020. Investigating surficial geologic controls on soil properties, inorganic nutrient uptake, and northern hardwood growth in Western Massachusetts. USA. J. Soil Sci. Plant Nut. 20 (3), 901–911. https://doi.org/10.1007/s42729-020-00176-3.

Marklund, L.G., 1988. Biomass Functions pine, Spruce and Birch in Sweden. Department of Forest Survey, Swedish University of Agricultural Sciences, Uppsala, Sweden.

Misson, L., Baldocchi, D.D., Black, T.A., Blanken, P.D., Brunet, Y., Yuste, Curiel, J, Dorsey, J.R, Falk, M, Granier, A, Irvine, M.R, Jarosz, N, Lamaud, E, Launiainen, S, Law, B.E, Longdoz, B, Loustau, D, McKay, M, Paw U, K.T, Vesala, T, Vickers, D, Wilson, K.B, Goldstein, A.H, 2007. Partitioning forest carbon fluxes with overstory and understory eddy-covariance measurements: a synthesis based on FLUXNET data. Agr. Forest Meteorol. 144 (1), 14–31. https://doi.org/10.1016/j.agrformet.2007.01.006.

Morén, A.-.S., Lindroth, A., 2000. CO2 exchange at the floor of a boreal forest. Agr. Forest Meteorol. 101 (1), 1–14. https://doi.org/10.1016/S0168-1923(99)00160-4.

Nilsson, M.-.C., Wardle, D.A., 2005. Understory vegetation as a forest ecosystem driver: evidence from the northern Swedish boreal forest. Front. Ecol. Environ. 3 (8), 421–428. https://doi.org/10.1890/1540-9295, 2005003[0421:UVAAFE]2.0.CO;2.

Nilsson, T., Lundin, L., 2006. Prediction of Bulk Density in Swedish forest Soils from the Organic Carbon Content and Soil Depth. Department of Forest Soils, Swedish University of Agricultural Sciences, Uppsala, Sweden.

Palmroth, S., Bach, L.H., Lindh, M., Kolari, P., Nordin, A., Palmqvist, K., 2019. Nitrogen supply and other controls of carbon uptake of understory vegetation in a boreal *Picea abies* forest. Agr. Forest Meteorol. 276–277. https://doi.org/10.1016/j.agrformet.2019.107620, 107620.

Pan, Y., Birdsey, R.A., Fang, J., Houghton, R., Kauppi, P.E., Kurz, W.A., Phillips, O.L., Shvidenko, A., Lewis, S.L., Canadell, J.G., Ciais, P., Jackson, R.B., Pacala, S.W., McGuire, A.D., Piao, S., Rautiainen, A., Sitch, S., Hayes, D., 2011. A large and persistent carbon sink in the world's forests. Science 333 (6045), 988–993. https://doi.org/10.1126/science.1201609.

Peichl, M., Sonnentag, O., Nilsson, M.B., 2015. Bringing color into the picture: using digital repeat photography to investigate phenology controls of the carbon dioxide exchange in a boreal mire. Ecosystems 18 (1), 115–131. https://doi.org/10.1007/s10021-014-9815-z.

Petersson, H., Ståhl, G., 2006. Functions for below-ground biomass of *Pinus sylvestris, Picea abies, Betula pendula* and *Betula pubescens* in Sweden. Scand. J. Forest Res. 21 (S7), 84–93. https://doi.org/10.1080/14004080500486864.

Petersson, L., Holmström, E., Lindbladh, M., Felton, A., 2019. Tree species impact on understory vegetation: vascular plant communities of Scots pine and Norway spruce managed stands in northern. Europe. Forest Ecol. Manag. 448, 330–345. https://doi.org/10.1016/j.foreco.2019.06.011.

Poorter, H., Niklas, K.J., Reich, P.B., Oleksyn, J., Poot, P., Mommer, L., 2012. Biomass allocation to leaves, stems and roots: meta-analyses of interspecific variation and environmental control. New Phytol 193 (1), 30–50. https://doi.org/10.1111/j.1469-8137.2011.03952.x.

Pregitzer, K.S., Euskirchen, E.S., 2004. Carbon cycling and storage in world forests: biome patterns related to forest age. Glob. Change Biol. 10 (12), 2052–2077. https://doi.org/10.1111/j.1365-2486.2004.00866.x.

Pumpanen, J., Kulmala, L., Lindén, A., Kolari, P., Nikinmaa, E., Hari, P., 2015. Seasonal dynamics of autotrophic respiration in boreal forest soil estimated by continuous chamber measurements. Boreal Environ. Res. 20, 637–650.

Repola, J., 2008. Biomass equations for birch in Finland. Silva Fenn 42 (4), 236.

Ryhti, K., Kulmala, L., Pumpanen, J., Isotalo, J., Pihlatie, M., Helmisaari, H.-.S., Leppälammi-Kujansuu, J., Kieloaho, A.-.J., Bäck, J., Heinonsalo, J., 2021. Partitioning of forest floor CO_2 emissions reveals the belowground interactions between different plant groups in a Scots pine stand in southern Finland. Agr. Forest Meteorol. 297, 108266 https://doi.org/10.1016/j.agrformet.2020.108266.

Saiz, G., Byrne, K.A., Butterbach-Bahl, K., Kiese, R., Blujdea, V., Farrell, E.P., 2006. Stand age-related effects on soil respiration in a first rotation Sitka spruce chronosequence in central Ireland. Glob. Change Biol. 12 (6), 1007–1020. https://doi.org/10.1111/j.1365-2486.2006.01145.x.

Sandström, F., Petersson, H., Kruys, N., Ståhl, G., 2007. Biomass conversion factors (density and carbon concentration) by decay classes for dead wood of *Pinus sylvestris, Picea abies* and *Betula* spp. in boreal forests of Sweden. Forest Ecol. Manag. 243 (1), 19–27. https://doi.org/10.1016/j.foreco.2007.01.081.

Sonnentag, O., Hufkens, K., Teshera-Sterne, C., Young, A.M., Friedl, M., Braswell, B.H., Milliman, T., O'Keefe, J., Richardson, A.D., 2012. Digital repeat photography for phenological research in forest ecosystems. Agr. Forest Meteorol. 152, 159–177. https://doi.org/10.1016/j.agrformet.2011.09.009.

Stendahl, J., Lundin, L., Nilsson, T., 2009. The stone and boulder content of Swedish forest soils. CATENA 77 (3), 285–291. https://doi.org/10.1016/j.catena.2009.02.011.

Street, L.E., Subke, J.-.A., Sommerkorn, M., Sloan, V., Ducrotoy, H., Phoenix, G.K., Williams, M., 2013. The role of mosses in carbon uptake and partitioning in arctic vegetation. New Phytol 199 (1), 163–175. https://doi.org/10.1111/nph.12285.

Stroeven, A.P., Hättestrand, C., Kleman, J., Heyman, J., Fabel, D., Fredin, O., Goodfellow, B.W., Harbor, J.M., Jansen, J.D., Olsen, L., Caffee, M.W., Fink, D., Lundqvist, J., Rosqvist, G.C., Strömberg, B., Jansson, K.N., 2016. Deglaciation of Fennoscandia. Quaternary Sci. Rev. 147, 91–121. https://doi.org/10.1016/j.quascirev.2015.09.016.

Thornley, J.H.M., Johnson, I.R., 1990. Plant and Crop modeling: A mathematical Approach to Plant and Crop Physiology. The Blackburn Press, Caldwell, New Jersey, NJ, USA, p. 669.

Ťupek, B., Minkkinen, K., Kolari, P., Starr, M., Chan, T., Alm, J., Vesala, T., Laine, J., Nikinmaa, E., 2008. Forest floor versus ecosystem CO_2 exchange along boreal ecotone between upland forest and lowland mire. Tellus B 60 (2), 153–166. https://doi.org/10.1111/j.1600-0889.2007.00328.x.

Vargas, R., Carbone, M.S., Reichstein, M., Baldocchi, D.D., 2011. Frontiers and challenges in soil respiration research: from measurements to model-data integration. Biogeochemistry 102 (1), 1–13. https://doi.org/10.1007/s10533-010-9462-1.

Vicca, S., Luyssaert, S., Peñuelas, J., Campioli, M., Chapin III, F.S., Ciais, P., Heinemeyer, A., Högberg, P., Kutsch, W.L., Law, B.E., Malhi, Y., Papale, D., Piao, S.L., Reichstein, M., Schulze, E.D., Janssens, I.A., 2012. Fertile forests produce biomass more efficiently. Ecol. Lett. 15 (6), 520–526. https://doi.org/10.1111/j.1461-0248.2012.01775.x.

Widén, B., 2002. Seasonal variation in forest-floor CO_2 exchange in a Swedish coniferous forest. Agr. Forest Meteorol. 111 (4), 283–297. https://doi.org/10.1016/S0168-1923(02)00026-6.

Yuan, Z.Y., Chen, H.Y.H., 2010. Fine root biomass, production, turnover rates, and nutrient contents in boreal forest ecosystems in relation to species, climate, fertility, and stand age: literature review and meta-analyses. Cr. Rev. Plant Sci. 29 (4), 204–221. https://doi.org/10.1080/07352689.2010.483579.

Zhang, Y., Xu, M., Chen, H., Adams, J., 2009. Global pattern of NPP to GPP ratio derived from MODIS data: effects of ecosystem type, geographical location and climate. Glob. Ecol. Biogeogr. 18 (3), 280–290. https://doi.org/10.1111/j.1466-8238.2008.00442.x.